Western University
Scholarship@Western

Chemistry Publications | Chemistry Department

Winter 12-9-2015

Group 6 Metal Pentacarbonyl Complexes of Air-Stable Primary, Secondary, and Tertiary Ferrocenylethylphosphines

Amir Rabiee Kenaree

Ethan R. Sauvé

Paul J. Ragogna

Joe Gilroy
jgilroy5@uwo.ca

Follow this and additional works at: https://ir.lib.uwo.ca/chempub

Part of the Chemistry Commons

Citation of this paper:

Rabiee Kenaree, Amir; Sauvé, Ethan R.; Ragogna, Paul J.; and Gilroy, Joe, "Group 6 Metal Pentacarbonyl Complexes of Air-Stable Primary, Secondary, and Tertiary Ferrocenylethylphosphines" (2015). *Chemistry Publications*. 71.
https://ir.lib.uwo.ca/chempub/71

Please do not adjust margins

Dalton Transactions

ARTICLE

Group 6 Metal Pentacarbonyl Complexes of Air-Stable Primary, Secondary, and Tertiary Ferrocenylethylphosphines

Received 00th January 20xx,
Accepted 00th January 20xx

DOI: 10.1039/x0xx00000x

www.rsc.org/

Amir Rabiee Kenaree, Ethan R. Sauvé, Paul J. Ragogna and Joe B. Gilroy*

The synthesis and characterization of a series of Group 6 metal pentacarbonyl complexes of air stable primary, secondary, and tertiary phosphines containing ferrocenylethyl substituents are reported [$M(CO)_5L$: M = Cr, Mo, W; L = $PH_2(CH_2CH_2Fc)$, $PH(CH_2CH_2Fc)_2$, $P(CH_2CH_2Fc)_3$]. The structure and composition of the complexes were confirmed by multinuclear NMR spectroscopy, IR and UV-Vis absorption spectroscopy, mass spectrometry, X-ray crystallography, and elemental analysis. The solid-state structural data reported revealed trends in M-C and M-P bond lengths that mirrored those of the atomic radii of the Group 6 metals involved. UV-Vis absorption spectroscopy and cyclic voltammetry highlighted characteristics consistent with electronically isolated ferrocene units including wavelengths of maximum absorption between 435 and 441 nm and reversible one-electron (per ferrocene unit) oxidation waves between 10 and –5 mV relative to the ferrocene/ferrocenium redox couple. IR spectroscopy confirmed that the σ donating ability of the phosphines increased as ferrocenylethyl substituents were introduced and that the tertiary phosphine ligand described is a stronger σ donor than PPh_3 and a weaker σ donor than PEt_3, respectively.

Introduction

Phosphines, including examples based on ferrocene,[1] are among the most widely exploited L-type ligands within the field of coordination chemistry[2,3] as a result of their tunable steric[4] and electronic[5] properties. They have been employed extensively as ancillary and/or labile ligands in homogeneous catalysts [*e.g.*, Grubbs I **1**, $Ni(dppp)Cl_2$ **2**, $Pd(dppf)Cl_2$ **3**, Wilkinson's catalyst $Rh(PPh_3)_3Cl$, and $Pd(PPh_3)_4$] that rapidly facilitate polymerization,[6] C-C and C-E bond formation,[7] and hydrogenation reactions.[8] While homogeneous catalysts commonly employ tertiary phosphines, relatively few examples include electron-rich primary and secondary alkyl phosphines due to their high reactivity towards air and moisture.

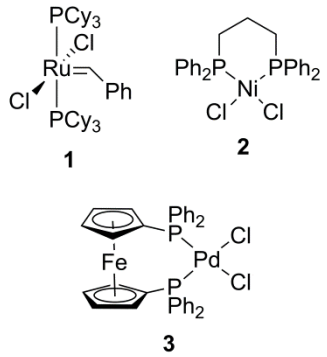

Building on recent advances surrounding the design and synthesis of air-stable primary, secondary, and tertiary phosphines[9,10] we have developed a unique series of electron-rich alkylphosphines bearing ferrocenylethyl and ruthenocenylethyl substituents (*e.g.*, **4a–c**).[11] These phosphines have shown utility as precursors to highly-metallized polymers[11a] and polymer networks[12] and in the phosphane-ene reaction.[13] They are remarkably stable towards air and moisture, redox active, and afford the ability to tune their steric properties through the sequential addition of ethylmetallocene units. Herein, we present a comprehensive study of the structure, bonding, and properties of a series of Group 6 metal pentacarbonyl (M = Cr, Mo, W) complexes of primary, secondary, and tertiary ferrocenylethylphosphines in order to establish fundamental knowledge of their ligand characteristics. Specifically, these ligands may be particularly well suited for the generation of high nuclearity transition metal clusters, where the presence of ferrocene has previously led to materials with application as sensors and electrode materials.[14]

Department of Chemistry and the Centre for Advanced Materials and Biomaterials Research (CAMBR), The University of Western Ontario, 1151 Richmond St. N., London, Ontario, Canada, N6A 5B7. Tel: +1-519-661-2111 ext. 81561, E-mail: joe.gilroy@uwo.ca.

Electronic Supplementary Information (ESI) available: NMR and UV-Vis absorption spectra, cyclic voltammograms, and solid-state structures. See DOI: 10.1039/x0xx00000x

Please do not adjust margins

Please do not adjust margins

Results and discussion

Synthesis and NMR spectroscopy

Primary, secondary, and tertiary ferrocenylethyl phosphines **4a–c** were prepared according to published protocols.[11] Monosubstituted phosphine complexes of Group 6 metal pentacarbonyls [$M(CO)_5$, M = Cr, Mo, W] were produced by first irradiating commercially available hexacarbonyls in THF with UV light to produce the corresponding THF adducts. The THF adducts were stirred with the appropriate phosphines for 2 h, isolated, and purified via column chromatography to afford phosphine complexes **5a–c** (M = Cr), **6a–c** (M = Mo), and **7a–c** (M = W) in yields ranging from 78 to 90% (Scheme 1). The structure and purity of the reported complexes were confirmed using multinuclear NMR spectroscopy, X-ray crystallography, IR and UV-Vis absorption spectroscopy, mass spectrometry, and elemental analysis.

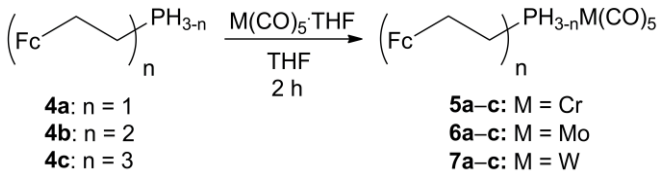

Scheme 1 Synthesis of primary, secondary, and tertiary phosphine-$M(CO)_5$ complexes **5a–c**, **6a–c**, and **7a–c**. Fc = ferrocene.

The NMR spectra of phosphine-$M(CO)_5$ complexes **5a–c**, **6a–c**, and **7a–c** were consistent with the proposed structures of the complexes, with each phosphine coordinated to a single $M(CO)_5$ fragment (Fig. 1, Figs. S1–S33, and Table 1). The ^{1}H NMR spectra of the complexes confirmed the presence of ligated primary, secondary, and tertiary phosphines and gave rise to two resonances (1.97–2.26 ppm and 2.51–2.77 ppm) attributed to the ethyl linker and a singlet and pair of *pseudo* triplets (4.04–4.26 ppm) due to the presence monosubstituted ferrocene groups. The phosphine protons were observed as complex doublets between 4.24 and 4.55 ppm for primary phosphine complexes **5a**, **6a**, and **7a** and between 4.52 and 4.85 for secondary phosphine complexes **5b**, **6b**, and **7b**.

^{31}P NMR spectroscopy showed that the phosphorus atoms within the phosphine-$M(CO)_5$ complexes described became increasingly deshielded as the number of ferrocenylethyl groups was increased (*e.g.*, **7a**: –101.9 ppm; **7b**: –43.6 ppm; and **7c**: –6.8 ppm). A second trend emerged when we

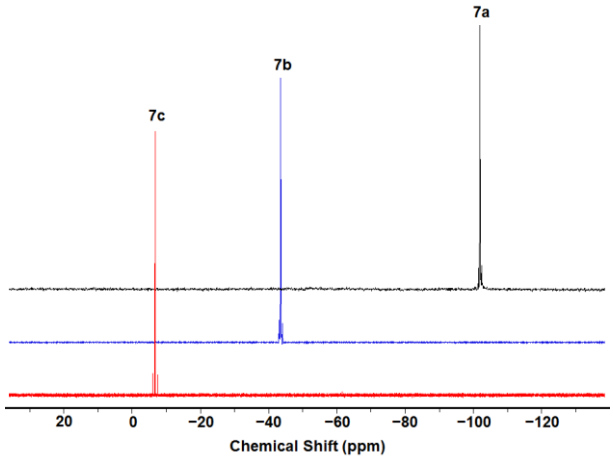

Fig. 1 $^{31}P\{^1H\}$ NMR spectra of primary, secondary, and tertiary phosphine-$W(CO)_5$ complexes **7a** (black line), **7b** (blue line), and **7c** (red line) recorded in $CDCl_3$.

examined the effect of the transition metal on the ^{31}P NMR shift. The shielding effect of the metals increased as we moved down Group 6 from Cr to W, resulting in a dramatic upfield shift of the ^{31}P NMR signals (*e.g.*, **5a**: –47.7 ppm; **6a**: –80.4 ppm; and **7a**: –101.9 ppm). The ^{13}C NMR signals observed for the CO ligands in each complex follow the same trend, with the most upfield resonances being observed for $W(CO)_5$ complexes and the most downfield resonances being observed for the $Cr(CO)_5$ complexes. Coupling to ^{183}W ($^1J_{PW}$ for **7a**: 217 Hz; **7b**: 225 Hz; and **7c**: 233 Hz) in complexes **7a–c** further supports the proposed structures of the complexes and the static nature of the P-W bonds (Figs. S27, S30, and S33). The observed trend for the P-W coupling constants is consistent with previous reports where a linear relationship between CO stretching frequencies (E mode) and coupling constants was established (Table 1).[15]

X-ray crystallography

The solid-state structures of complexes **5c**, **6c**, and **7a–c** were determined by single crystal X-ray diffraction and are shown in Figs. 2, S34, and S35 and the data are summarized in Table 2. The structures contain many general features including a group 6 metal in an octahedral environment, C-O bond lengths between 1.138(3) and 1.145(4) Å, and P-C bond

Table 1 Selected characterization data for complexes **5a–c**, **6a–c**, and **7a–c**.

	5a	5b	5c	6a	6b	6c	7a	7b	7c
υ(CO) A_{1cis} [a]	2067	2062	2058	2075	2071	2067	2074	2070	2066
υ(CO) A_{1trans} [a]	1979	1979	1975	1993	1986	1981	1976	1978	1974
υ(CO) E [a]	1916	1916	1922	1922	1925	1929	1912	1914	1922
^{31}P (δ) [b]	–47.7	3.5	30.4	–80.4	–22.9	12.5	–101.9	–43.6	–6.8
$^1J_{PH}$ (Hz) [b]	324	321	-	319	315	-	333	328	-
$^1J_{PW}$ (Hz) [b]	-	-	-	-	-	-	217	225	233
$E_{1/2}$ (mV) [c]	10	0	–5	10	0	–5	10	0	–5
λ_{max} (nm) [d]	437	436	439	439	436	435	441	437	436
ε (M^{-1} cm^{-1}) [d]	130	230	350	115	250	350	120	245	335

[a]Recorded as thin films on KBr plates. [b]Recorded in $CDCl_3$. [c]Recorded at scan rates of 250 mV s^{-1} in 1 mM degassed 2:1 CH_2Cl_2:CH_3CN solutions containing 0.1 M [*n*-Bu_4N][SO_3CF_3] as supporting electrolyte and referenced relative to the ferrocene/ferrocenium redox couple. [d]Recorded in CH_2Cl_2.

This journal is © The Royal Society of Chemistry 20xx

Please do not adjust margins

Please do not adjust margins

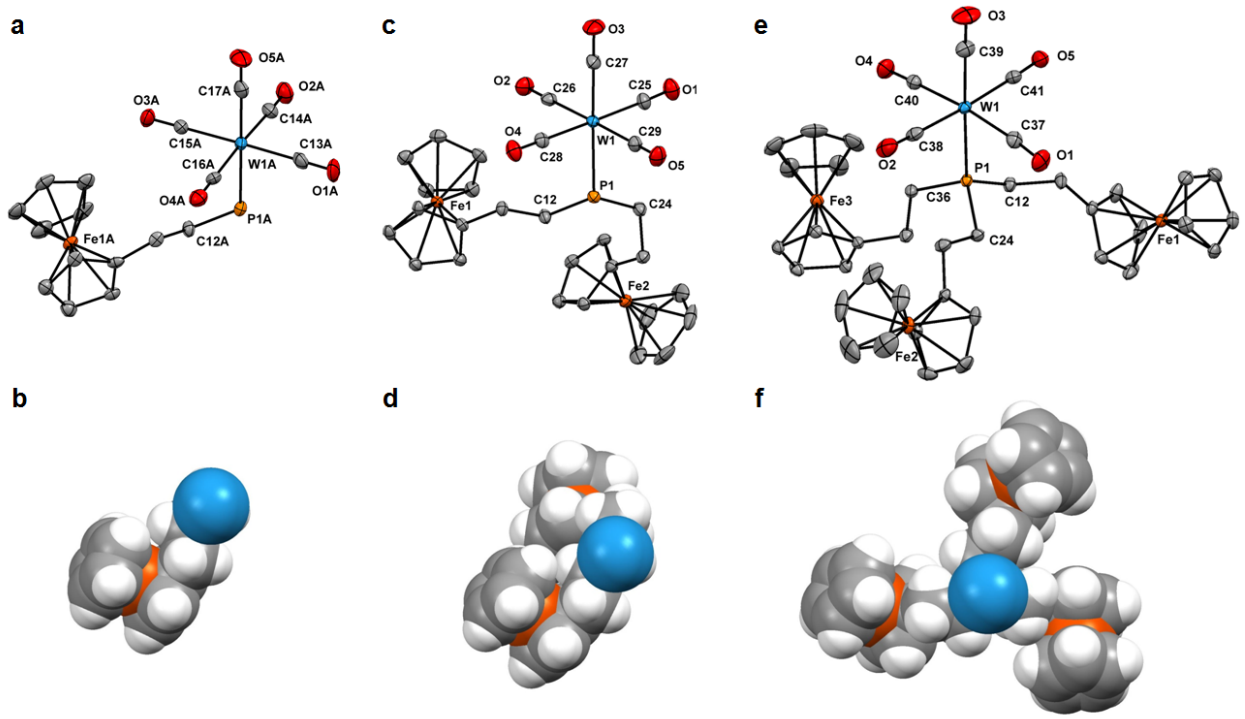

Fig. 2 Solid-state structures and partial spacefill models of primary, secondary, and tertiary phosphine-W(CO)$_5$ complexes **7a** (a,b), **7b** (c,d), and **7c** (e,f). Anisotropic displacement ellipsoids are shown at 50% probability and hydrogen atoms have been omitted for clarity. Only one of the two structurally similar molecules from the asymmetric unit for **7a** is shown.

Table 2 Selected bond lengths (Å) and angles for complexes **5c**, **6c**, and **7a–c**.

	5c	**6c**	**7a**[a]	**7b**	**7c**
trans M-C	1.866(4)	2.018(4)	2.012(8)	1.998(4)	2.012(2)
cis M-C (avg)	1.895(4)	2.041(4)	2.044(8)	2.047(5)	2.041(3)
M-C (avg)	1.890(4)	2.036(4)	2.038(8)	2.037(5)	2.035(3)
M-P	2.3747(10)	2.5121(11)	2.492(2)	2.5135(10)	2.5094(8)
trans C-O	1.149(4)	1.141(4)	1.145(8)	1.156(5)	1.141(3)
cis C-O (avg)	1.145(4)	1.144(4)	1.143(8)	1.136(6)	1.138(3)
C-O (avg)	1.145(4)	1.144(4)	1.144(8)	1.140(6)	1.138(3)
P-C (avg)	1.832(3)	1.833(3)	1.842(7)	1.832(4)	1.832(2)
C-P-C (avg)	102.28(15)	102.46(16)	-	104.57(19)	102.62(10)

[a]The asymmetric unit for **7a** contains two crystallographically independent molecules. Average values for the two molecules are listed.

lengths of 1.832(3)–1.842(7) Å. The P-C bond lengths observed were slightly shorter than those of free phosphines **4a–c** [1.843(1)–1.93(1) Å].[11a]

Examination of the solid-state structures of **7a–c** (M = W) allowed for direct comparison of the primary, secondary, and tertiary phosphine complexes. Partial space filling models, viewed down the W-P bond axis, are shown in Fig. 2 and demonstrate the dramatic increase in relative size associated with the sequential addition of ferrocenylethyl substituents at phosphorus. The M-P distances are 2.492(2) Å for **7a**, 2.5135(10) Å for **7b**, and 2.5094(8) Å for **7c**, which provides an indication that the introduction of additional ferrocenylethyl substituents at phosphorus does not result in a significant enhancement in the steric interactions between the phosphine ligands and M(CO)$_5$ unit. A further indication that the structures of the phosphine ligands are not being altered in the complexes due to unfavorable steric interactions are the average C-P-C angles, which increased from 99.03(4)° and 99.68(6)° in free phosphines **4b** and **4c** to 104.57(19)° and 102.62(10)° in their respective W(CO)$_5$ complexes, **7b** and **7c**.

By comparing the solid-state structures of tertiary phosphine complexes **5c**, **6c**, and **7c** we assessed the influence of the different Group 6 metals on their structural metrics. The M-P bond length observed for complex **5c** [M = Cr, 2.3747(10) Å] was shorter than that of **6c** [M = Mo, 2.5121(11) Å] due to an increase in the number of electrons associated with a change from Period 4 to Period 5. Similar elongation of the M-P bond was not observed when Mo was replaced by W in **7c** [2.5094(8) Å] due to the lanthanoid contraction.

Please do not adjust margins

Please do not adjust margins

FT-IR spectroscopy

The assignment of the CO stretching frequencies [υ(CO)] of monosubstituted metal carbonyl complexes [$M(CO)_5L$] and surrounding theory was developed by Orgel and Cotton in the early 1960s.[16] Based on their findings, we expected to observe three unique CO stretches (A_{1cis}, A_{1trans}, E) in the IR spectra of phosphine-$M(CO)_5$ complexes **5a–c**, **6a–c**, and **7a–c** (Fig. 3, Figs. S36–S44, and Table 1). In general, the υ(CO) A_{1cis} (2058–2075 cm^{-1}) and A_{1trans} (1974–1993 cm^{-1}) absorptions for the complexes were shown to decrease when primary phosphine **4a** was replaced by secondary phosphine **4b** and when secondary phosphine **4b** was replaced by tertiary phosphine **4c**. This trend provides evidence that the σ donating ability of the phosphine ligands employed in this study, and thus the extent of π backbonding to CO, increased as ferrocenylethyl substituents were introduced at the ligand. By comparing the CO stretching frequencies [υ(CO) A_{1trans}] observed for tertiary phosphine complexes **5c**, **6c**, and **7c** with those recorded for analogous PEt_3 (Et_3PCrCO_5: 1943 cm^{-1}; Et_3PMoCO_5: 1944 cm^{-1}; Et_3PWCO_5: 1943 cm^{-1})[17] and PPh_3 (Ph_3PCrCO_5: 1989 cm^{-1}; Ph_3PMoCO_5: 1990 cm^{-1}; Ph_3PWCO_5: 1981 cm^{-1})[16b] complexes, we conclude that the tertiary phosphine ligand employed in this study is a stronger σ donor than the phenyl-substituted analog, but a weaker σ donor than the ethyl-substituted analog.

Variation of the transition metals involved provided further insight into the bonding within the series of complexes. The extent of π backbonding to the CO ligands, based on the values of υ(CO) A_{1trans} and A_{1cis}, followed the trend: Cr > W > Mo and mirrored the trend in electronegativities for the metals involved.

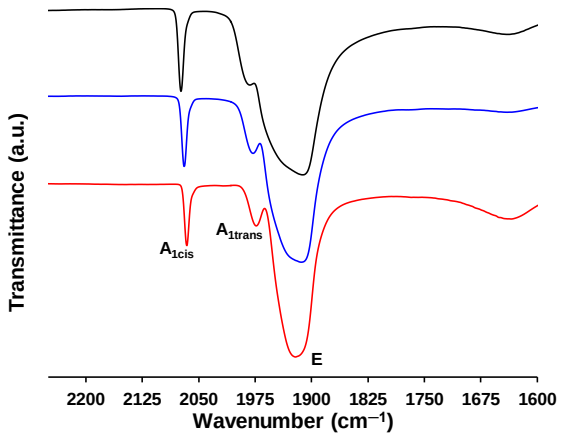

Fig. 3 FT-IR spectra (CO region) for primary, secondary, and tertiary phosphine-$W(CO)_5$ complexes **7a** (black line), **7b** (blue line), and **7c** (red line) recorded as thin films on KBr plates.

UV-Vis absorption spectroscopy and cyclic voltammetry

The UV-Vis absorption spectra and cyclic voltammograms (CVs) recorded for phosphine-$M(CO)_5$ complexes **5a–c**, **6a–c**, and **7a–c** were consistent with the presence of electronically isolated ferrocene groups. Due to the large octahedral field splitting associated with strong field carbonyl ligands, the UV-Vis absorption spectra of phosphine-$M(CO)_5$ complexes **5a–c**, **6a–c**, and **7a–c** in CH_2Cl_2 are comprised primarily of features associated with the ferrocene moieties (Fig. 4, Figs. S45–S50, and Table 1). For each series of primary, secondary, and tertiary complexes the molar absorptivity (ε) at the absorption maxima (λ_{max} = 435–441 nm) associated with the formally forbidden, d→d transitions of ferrocene scaled linearly with the number of ferrocene groups present and ranged from 115 to 350 M^{-1} cm^{-1}.

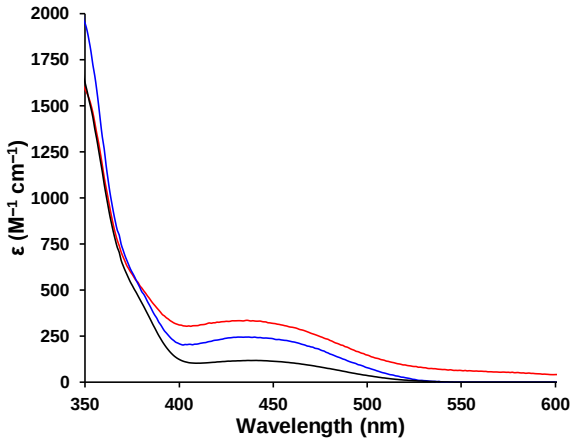

Fig. 4 UV-Vis spectra of primary, secondary, and tertiary phosphine-$W(CO)_5$ complexes **7a** (black line), **7b** (blue line), and **7c** (red line) recorded in CH_2Cl_2.

The electrochemical properties of phosphine-$M(CO)_5$ complexes **5a–c**, **6a–c**, and **7a–c** were studied by collecting CVs of 1 mM degassed 2:1 CH_2Cl_2:CH_3CN solutions containing 0.1 M [*n*-Bu_4N][SO_3CF_3] as supporting electrolyte (Fig. 5, Figs. S51–S58, and Table 1). This solvent/supporting electrolyte combination was required in order to solubilize both the ferrocene and electrogenerated ferrocenium forms of the complexes. When traditional electrolytes (*e.g.*, [*n*-Bu_4N][PF_6]) were employed in non-polar solvents such as CH_2Cl_2, plating of the ferrocenium forms of the complexes resulted in a loss of diffusion control at the interface of the working electrode. For each complex a single reversible oxidation wave with peak currents corresponding to one electron per ferrocene unit was observed. Significantly, the small electrochemical feature observed at *ca.* –150 mV vs. Fc/Fc^+ in the CVs of the free phosphines (Fig. 5), which has been previously linked to the presence of the phosphorus lone pair,[11] disappears upon metal coordination. Within each series complexes the relatively electron-poor primary phosphine complexes (10 mV) were harder to oxidize than the secondary phosphine complexes which contain an additional ferrocenylethyl substituent (0 mV). Furthermore, the relatively electron-rich tertiary phosphine complexes were the easiest to oxidize (–5 mV). All of the complexes reported in this study were more difficult to oxidize than free phosphines **4a–c** under identical conditions[11a] and there were no observable differences in the CVs when the transition metals were varied.

This journal is © The Royal Society of Chemistry 20xx

Please do not adjust margins

Please do not adjust margins

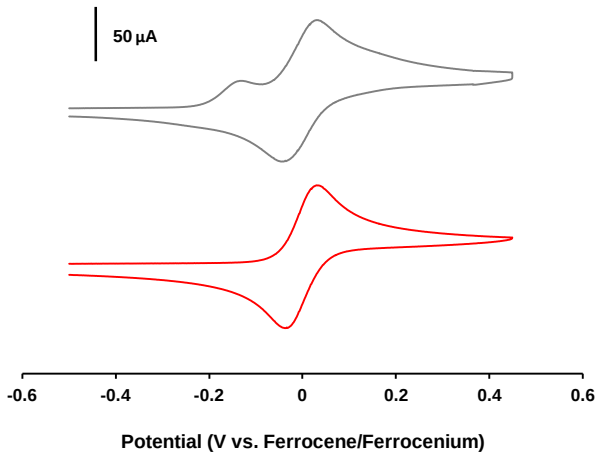

Fig. 5 Cyclic voltammograms of tertiary phosphine **4c** (grey line) and tertiary phosphine-W(CO)$_5$ complex **7c** (red line) recorded at 250 mV s^{-1} for 1 mM degassed 2:1 CH_2Cl_2:CH_3CN solutions containing 0.1 M [*n*-Bu_4N][SO_3CF_3] as supporting electrolyte.

Conclusions

We have reported the synthesis and characterization of a series of Group 6 M(CO)$_5$ complexes of air-stable, redox-active primary, secondary, and tertiary ferrocenylethylphosphines. ^{31}P NMR spectroscopic studies confirmed the phosphine units to be intact in the complexes while X-ray crystallography was used to verify the proposed structures of the complexes and demonstrated trends in M-C and M-P bond lengths that followed those of the atomic radii of the metals involved. The X-ray structures of complexes **7a–c** also allowed for a qualitative assessment of the relative size of the ligands, showing that the volume occupied by the phosphine ligands increased dramatically with the sequential introduction of additional ferrocenylethyl substituents. UV-Vis absorption spectroscopy and cyclic voltammetry studies confirmed that the ferrocene moieties were electronically isolated from the metals in the complexes studied, and revealed properties consistent with monosubstituted ferrocenes. By monitoring the CO stretches of the complexes with IR spectroscopy, we demonstrated that the σ donating ability of the phosphine ligands increased as ferrocenylethyl substituents were introduced [σ donor strength: P(CH_2CH_2Fc)$_3$ > PH(CH_2CH_2Fc)$_2$ > PH_2(CH_2CH_2Fc)] and that the σ donating ability of the phosphines were intermediate between those of ethyl and phenyl phosphines [σ donor strength: PEt_3 > P(CH_2CH_2Fc)$_3$ > PPh_3].

Based on the fundamental knowledge of the ligand characteristics of this promising class of ferrocenylethyl phosphine ligands produced as a result of this work, we are hopeful that they will be employed by those working towards novel homogeneous catalysts and redox-active coordination complexes. Our future work in this area will focus on their use in the coordination chemistry of late transition metal chalcogens as we pursue large, redox-active transition metal clusters.

Experimental section

General considerations

All reactions and manipulations were carried out under a nitrogen atmosphere using standard glove box or Schlenk techniques unless otherwise stated. Solvents were obtained from Caledon Laboratories, dried using an Innovative Technologies Inc. solvent purification system, collected under vacuum, and stored under a nitrogen atmosphere over 4 Å molecular sieves. All reagents were purchased from Sigma-Aldrich or Alfa Aesar and used as received, aside from metal carbonyls which were sublimed before use. Primary, secondary, and tertiary phosphines **4a–c** were synthesized according to previously reported protocols.[11] UV irradiation experiments were conducted with a medium pressure mercury lamp in a Quartz housing with reaction flasks mounted approximately 10 cm from the lamp. ^{1}H, ^{13}C, and ^{31}P NMR spectra were recorded on a 600 MHz (^{1}H: 599.5 MHz, ^{13}C: 150.8 MHz, ^{31}P: 242.6 MHz) Varian INOVA instrument. ^{1}H NMR spectra were referenced to residual $CHCl_3$ (7.27 ppm) and ^{13}C{^{1}H} NMR spectra were referenced to $CDCl_3$ (77.0 ppm). ^{31}P NMR spectra were referenced to PPh_3, as an internal standard (–6.0 ppm relative to H_3PO_4). Mass spectrometry data were recorded in positive-ion mode using a high resolution Finnigan MAT 8400 spectrometer. UV-Vis spectra were recorded using a Cary 300 Scan instrument. Infrared spectra were recorded using a PerkinElmer Spectrum Two FT-IR spectrometer as thin films on KBr plates. Elemental analyses (C and H) were carried out by Laboratoire d'Analyse Élémentaire de l'Université de Montréal, Montréal, QC, Canada.

Cyclic voltammetry

CVs were collected using a Bioanalytical Systems Inc. (BASi) Epsilon potentiostat and analyzed using BASi Epsilon software. Typical electrochemical cells consisted of a three-electrode setup including a glassy carbon working electrode, platinum wire counter electrode, and silver wire *pseudo*-reference electrode. Experiments were run at a scan rate of 250 mV s^{-1} in degassed 2:1 CH_2Cl_2:CH_3CN solutions of the analyte (~1 mM) and supporting electrolyte (0.1 M [*n*-Bu_4N][SO_3CF_3]) under a blanket of argon. CVs were referenced relative to a decamethylferrocene internal standard (1 mM, –520 mV relative to ferrocene/ferrocenium under identical conditions) and corrected for internal cell resistance using the BASi Epsilon software.

X-ray crystallography

Single crystals of **5c**, **7b**, and **7c** suitable for X-ray diffraction studies were grown by slow evaporation of concentrated Et_2O solutions. Crystals of **6c** were grown by slow diffusion of hexanes into a concentrated THF solution and crystals of **7a** were grown by slow diffusion of pentane into a concentrated

Please do not adjust margins

Please do not adjust margins

Table 3 Selected X-ray diffraction data collection and refinement details for complexes **5c**, **6c**, and **7a–c**.

	5c	**6c**	**7a**	**7b**	**7c**
Chemical formula	$C_{41}H_{39}CrFe_3O_5P$	$C_{41}H_{39}Fe_3MoO_5P$	$C_{17}H_{15}FeO_5PW$	$C_{29}H_{27}Fe_2O_5PW$	$C_{41}H_{39}Fe_3O_5PW$
FW (g mol^{-1})	862.24	906.18	569.96	782.02	994.09
Temp (K)	110	110	110	110	110
Crystal system	monoclinic	monoclinic	monoclinic	monoclinic	monoclinic
Crystal habit	orange prism	yellow prism	yellow plate	yellow prism	orange prism
Space group	C2/c	C2/c	$P2_1/c$	$P2_1/c$	C2/c
λ (Å)	1.54178	0.71073	0.71073	0.71073	0.71073
a (Å)	20.142(3)	20.300(8)	20.416(7)	17.504(2)	20.307(6)
b (Å)	15.184(2)	15.312(5)	7.239(3)	12.9315(14)	15.287(5)
c (Å)	25.001(6)	25.118(10)	25.066(9)	12.708(2)	25.101(7)
α (deg)	90	90	90	90	90
β (deg)	104.581(9)	104.367(10)	97.888(15)	109.260(5)	104.391(13)
γ (deg)	90	90	90	90	90
V (Å^3)	7400(2)	7563(5)	3669(2)	2715.5(6)	7548(4)
Z	8	8	8	4	8
ρ (g cm^{-3})	1.548	1.592	2.063	1.913	1.750
μ (cm^{-1})	12.369	1.538	7.166	5.377	4.254
R_1 [I > 2σ(I)]	0.0350	0.0312	0.0379	0.0412	0.0381
ωR_2 [I > 2σ(I)]	0.0772	0.0633	0.0631	0.0971	0.0688
R_1 (all data)	0.0460	0.0456	0.0615	0.0684	0.0670
ωR_2 (all data)	0.0818	0.0691	0.0686	0.1115	0.0757
GOF	1.045	1.042	1.063	1.019	1.062

$R_1 = \Sigma(|F_o| - |F_c|) / \Sigma F_o$, $\omega R_2 = [\Sigma(\omega(F_o^2 - F_c^2)^2) / \Sigma(\omega F_o^4)]^{½}$; GOF = $[\Sigma (\omega(F_o^2 - F_c^2)^2) / (\text{No. of reflns.} - \text{No. of params.})]^{½}$.

$CHCl_3$ solution. The samples were mounted on a MiTeGen polyimide micromount with a small amount of Paratone N oil. X-ray measurements for **6c** and **7a–c** were made on a Bruker ApexII CCD diffractometer. Measurements for **5c** were made on a Nonius KappaCCD ApexII diffractometer. The unit cell dimensions were determined from a symmetry constrained fit of 5928 reflections with 7.30° < 2θ < 121.36° for **5c**, 9131 reflections with 5.58° < 2θ < 46.98° for **6c**, 9155 reflections with 5.86° < 2θ < 49.02° for **7a**, 9530 reflections with 7.48° < 2θ < 64.96° for **7b**, and 9801 reflections with 5.58° < 2θ < 65.90° for **7c**. The data collection strategy was a number of ω and ϕ scans which collected data up to 121.410° (2θ) for **5c**, 47.242° (2θ) for **6c**, 50.758° (2θ) for **7a**, 72.758° (2θ) for **7b**, and 72.824° (2θ) for **7c**, respectively. The frame integration was performed using SAINT.[18] The resulting raw data were scaled and absorption corrected using a multi-scan averaging of symmetry equivalent data using SADABS,[19] except the data for **7b** which were processed using TWINABS.[20] The twin law for **7b** was derived from the two orientation matrices using the GNU Octave program[21] and was determined to be:

−0.986857	−0.045843	−0.154954
−0.045946	−0.839733	0.541052
−0.154923	0.541061	0.826590

which represents a 180° rotation about [1 −1 −1]. The twin fraction refined to a value of 0.44883(63). The structures for **5c**, **6c**, **7a**, **7b**, and **7c** were solved by using a dual space methodology using the SHELXT program.[22] All non-hydrogen atoms were obtained from the initial solution. The hydrogen atoms were introduced at idealized positions and were allowed to ride on the parent atom aside for **6c** where they were treated in a mixed fashion. The structural models were fit to the data using full matrix least-squares based on F^2. The calculated structure factors included corrections for anomalous dispersion from the usual tabulation. The structures were refined using the SHELXL-2014 program from the SHELX suite of crystallographic software.[23] For complex **7a**, the minor component of the rotational disorder associated with the unsubstituted Cp ligands could not be fully resolved (see .cif file for details). Graphic plots were produced using Mercury (v3.3). Structural data has been deposited in the CCDC (1423358–1423362). For additional collection and refinement details, see Table 3.

Representative procedure for the preparation of $M(CO)_5$ complexes of 5a–c, 6a–c, 7a–c.

Primary phosphine complex 5a (M = Cr)

$Cr(CO)_6$ (0.268 g, 1.22 mmol, 5 equiv.) was dissolved in 15 mL dry THF in a sealed 1 L Pyrex flask and irradiated with UV light for 2.5 h to produce an orange solution containing $Cr(CO)_5THF$. The flask was opened inside a glove box and a solution of **4a** (0.060 g, 0.244 mmol) in 15 mL dry THF was added dropwise over a 5 min period. The resulting solution was allowed to stir for 2 h before the solvent was removed under reduced pressure. The reaction mixture was combined with diethyl ether (5 mL) and the mixture filtered to remove excess $Cr(CO)_6$. The filtrate was then mixed with Celite, concentrated *in vacuo*, and transferred to the top of a silica column

 This journal is © The Royal Society of Chemistry 20xx

Please do not adjust margins

Please do not adjust margins

(1" × 4"). Using flash column chromatography and a gradient solvent strategy, residual $Cr(CO)_6$, and **5a** were separated. Using 4:1 hexanes:dichloromethane as eluent, **5a** (R_f = 0.36) was isolated from the column before $Cr(CO)_6$ was eluted using hexanes (R_f = 0.68). The solution containing **5a** was concentrated *in vacuo* to yield an orange solid. Yield = 0.090 g, 84%. M.p. 74–76 °C. ^{1}H NMR ($CDCl_3$): δ 4.28 (d of m, $^1J_{HP}$ = 324 Hz, 2H, PH_2), 4.14 (s, 5H, C_5H_5), 4.13 (s, 2H, β-C_5H_4R), 4.11 (s, 2H, α-C_5H_4R), 2.72 (m, 2H, $C_5H_4CH_2$), 2.04 (m, 2H, CH_2PH_2). $^{13}C\{^1H\}$ NMR ($CDCl_3$): δ 220.3 (d, $^2J_{CP}$ = 7 Hz, *cis*-CO), 216.0 (d, $^2J_{CP}$ = 14 Hz, *trans*-CO), 86.8 (d, $^3J_{CP}$ = 10 Hz, *ipso*-C_5H_4R), 68.6 (s, C_5H_5), 68.1 (s, α-C_5H_4R), 67.8 (s, β-C_5H_4R), 30.5 (d, $^2J_{CP}$ = 7 Hz, $C_5H_4CH_2$), 23.4 (d, $^1J_{CP}$ = 25 Hz, CH_2PH_2). ^{31}P NMR ($CDCl_3$): δ –47.7 (t of m, $^1J_{PH}$ = 324 Hz). FT-IR: 2329 (w), 2067 (m), 1979 (w), 1916 (s), 1105 (w), 1090 (w), 1000 (w), 926 (w), 821 (w), 674 (m), 649 (m) cm^{-1}. UV-Vis (CH_2Cl_2): λ_{max} 437 nm (ε = 130 M^{-1} cm^{-1}). Mass Spec. (EI, +ve mode): exact mass calculated for $[C_{17}H_{15}{}^{52}Cr^{56}FeO_5P]^+$: 437.9412; exact mass found: 437.9418; difference: +1.4 ppm. Anal. Calcd. (%) for $C_{17}H_{15}CrFeO_5P$: C, 46.60; H, 3.45. Found: C, 46.66; H, 3.47.

Secondary phosphine complex 5b (M = Cr)

From $Cr(CO)_6$ (0.240 g, 1.09 mmol, 5 equiv.) and phosphine **4b** (0.100 g, 0.218 mmol). Yield = 0.108 g, 80% of orange solid (R_f = 0.23). M.p. 88–90 °C. ^{1}H NMR ($CDCl_3$): δ 4.52 (d of m, $^1J_{HP}$ = 322 Hz, 1H, P*H*), 4.13 (s, 10H, C_5H_5), 4.12 (s, 4H, β-C_5H_4R), 4.11 (s, 4H, α-C_5H_4R), 2.63 (m, 4H, $C_5H_4CH_2$), 2.09 (m, 4H, CH_2PH). $^{13}C\{^1H\}$ NMR ($CDCl_3$): δ 220.7 (d, $^2J_{CP}$ = 7 Hz, *cis*-CO), 216.8 (d, $^2J_{CP}$ = 14 Hz, *trans*-CO), 87.4 (d, $^3J_{CP}$ = 13 Hz, *ipso*-C_5H_4R), 68.6 (s, C_5H_5), 67.8 (d, $^4J_{CP}$ = 16 Hz, α-C_5H_4R), 67.6 (s, β-C_5H_4R), 27.4 (d, $^1J_{CP}$ = 22 Hz, CH_2PH), 26.6 (d, $^2J_{CP}$ = 2 Hz, $C_5H_4CH_2$). ^{31}P NMR ($CDCl_3$): δ 3.5 (d of m, $^1J_{PH}$ = 321 Hz). FT-IR: 2922 (w), 2062 (m), 1979 (w), 1916 (s), 1637 (m), 1105 (w), 999 (w), 817 (w), 676 (w), 651 (w) cm^{-1}. UV-Vis (CH_2Cl_2): λ_{max} 436 nm (ε = 230 M^{-1} cm^{-1}). Mass Spec. (EI, +ve mode): exact mass calculated for $[C_{29}H_{27}{}^{52}Cr^{56}Fe_2O_5P]^+$: 649.9700; exact mass found: 649.9677; difference: –3.5 ppm. Anal. Calcd. (%) for $C_{29}H_{27}CrFe_2O_5P$: C, 53.57; H, 4.19. Found: C, 53.68; H, 4.24.

Tertiary phosphine complex 5c (M = Cr)

From $Cr(CO)_6$ (0.246 g, 1.12 mmol, 5 equiv.) and phosphine **4c** (0.150 g, 0.224 mmol). Yield = 0.145 g, 78% of orange solid (R_f = 0.14). M.p. 140–142 °C. ^{1}H NMR ($CDCl_3$): δ 4.18 (s, 15H, C_5H_5), 4.17 (s, 12H, α-C_5H_4R and β-C_5H_4R), 2.61 (m, 6H, $C_5H_4CH_2$), 2.08 (m, 6H, CH_2P). $^{13}C\{^1H\}$ NMR ($CDCl_3$): δ 220.9 (d, $^2J_{CP}$ = 7 Hz, *cis*-CO), 217.5 (d, $^2J_{CP}$ = 14 Hz, *trans*-CO), 87.9 (d, $^3J_{CP}$ = 15 Hz, *ipso*-C_5H_4R), 68.6 (s, C_5H_5), 67.7 (s, α-C_5H_4R), 67.6 (s, β-C_5H_4R), 30.6 (d, $^1J_{CP}$ = 18 Hz, CH_2P), 23.8 (s, $C_5H_4CH_2$). ^{31}P NMR ($CDCl_3$): δ 30.4 (m). FT-IR: 3092 (w), 2928 (w), 2058 (m), 1975 (w), 1922 (s), 1635 (w), 1411 (w), 1106 (w), 1000 (w), 818 (w), 755 (w), 677 (m), 655 (m) cm^{-1}. UV-Vis (CH_2Cl_2): λ_{max} 439 nm (ε = 350 M^{-1} cm^{-1}). Mass Spec. (EI, +ve mode): exact mass calculated for $[C_{41}H_{39}{}^{52}Cr^{56}Fe_3O_5P]^+$: 861.9988; exact mass found: 861.9966; difference: –2.6 ppm. Anal. Calcd. (%) for $C_{41}H_{39}CrFe_3O_5P$: C, 57.11; H, 4.56. Found: C, 57.11; H, 4.62.

Primary phosphine complex 6a (M = Mo)

From $Mo(CO)_6$ (0.322 g, 1.22 mmol, 5 equiv.) and phosphine **4a** (0.060 g, 0.244 mmol). Yield = 0.087 g, 79% of orange solid (R_f = 0.35). M.p. 56–58 °C. ^{1}H NMR ($CDCl_3$): δ 4.24 (d of m, $^1J_{HP}$ = 319 Hz, 2H, PH_2), 4.13 (s, 5H, C_5H_5), 4.12 (*pseudo*-t, $^3J_{HH}$ = 2 Hz, 2H, β-C_5H_4R), 4.11 (*pseudo*-t, $^3J_{HH}$ = 2 Hz, 2H, α-C_5H_4R), 2.70 (m, 2H, $C_5H_4CH_2$), 2.02 (m, 2H, CH_2PH_2). $^{13}C\{^1H\}$ NMR ($CDCl_3$): δ 208.7 (d, $^2J_{CP}$ = 23 Hz, *cis*-CO), 204.9 (d, $^2J_{CP}$ = 9 Hz, *trans*-CO), 86.9 (d, $^3J_{CP}$ = 10 Hz, *ipso*-C_5H_4R), 68.6 (s, C_5H_5), 68.1 (s, α-C_5H_4R), 67.7 (s, β-C_5H_4R), 30.6 (d, $^2J_{CP}$ = 5 Hz, $C_5H_4CH_2$), 23.2 (d, $^1J_{CP}$ = 25 Hz, CH_2PH_2). ^{31}P NMR ($CDCl_3$): δ –80.4 (t of m, $^1J_{PH}$ = 319 Hz). FT-IR: 3094 (w), 2917 (w), 2345 (w), 2075 (m), 1993 (w), 1922 (s), 1644 (w), 1413 (w), 1445 (w), 1105 (w), 1089 (w), 1000 (w), 925 (w), 670 (w), 607 (m) cm^{-1}. UV-Vis (CH_2Cl_2): λ_{max} 439 nm (ε = 115 M^{-1} cm^{-1}). Mass Spec. (EI, +ve mode): exact mass calculated for $[C_{17}H_{15}{}^{56}Fe^{92}MoO_5P]^+$: 477.9076; exact mass found: 477.9056; difference: –4.2 ppm. Anal. Calcd. (%) for $C_{17}H_{15}FeMoO_5P$: C, 42.36; H, 3.14. Found: C, 42.45; H, 2.99.

Secondary phosphine complex 6b (M = Mo)

From $Mo(CO)_6$ (0.288 g, 1.09 mmol, 5 equiv.) and phosphine **4b** (0.100 g, 0.218 mmol). Yield = 0.117 g, 81% of orange solid (R_f = 0.20). M.p. 64–66 °C. ^{1}H NMR ($CDCl_3$): δ 4.54 (d of m, $^1J_{HP}$ = 315 Hz, 1H, P*H*), 4.13 (s, 10H, C_5H_5), 4.11 (s, 8H, α-C_5H_4R, and β-C_5H_4R), 2.63 (m, 4H, $C_5H_4CH_2$), 2.05 (m, 4H, CH_2PH). $^{13}C\{^1H\}$ NMR ($CDCl_3$): δ 209.2 (d, $^2J_{CP}$ = 22 Hz, *cis*-CO), 205.7 (d, $^2J_{CP}$ = 9 Hz, *trans*-CO), 87.5 (d, $^3J_{CP}$ = 14 Hz, *ipso*-C_5H_4R), 68.6 (s, C_5H_5), 67.9 (d, $^4J_{CP}$ = 15 Hz, α-C_5H_4R), 67.6 (s, β-C_5H_4R), 27.6 (d, $^1J_{CP}$ = 22 Hz, CH_2PH), 27.0 (s, $C_5H_4CH_2$). ^{31}P NMR ($CDCl_3$): δ –22.9 (d of m, $^1J_{PH}$ = 315 Hz). FT-IR: 3094 (w), 2917 (w), 2071 (m), 1986 (w), 1925 (s), 1640 (w), 1411 (w), 1105 (w), 1000 (w), 819 (w), 608 (m) cm^{-1}. UV-Vis (CH_2Cl_2): λ_{max} 436 nm (ε = 250 M^{-1} cm^{-1}). Mass Spec. (EI, +ve mode): exact mass calculated for $[C_{29}H_{27}{}^{56}Fe_2{}^{92}MoO_5P]^+$: 689.9367; exact mass found: 689.9335; difference: –4.6 ppm. Anal. Calcd. (%) for $C_{29}H_{27}Fe_2MoO_5P$: C, 50.18; H, 3.92. Found: C, 50.25; H, 3.95.

Tertiary phosphine complex 6c (M = Mo)

From $Mo(CO)_6$ (0.296 g, 1.12 mmol, 5 equiv.) and phosphine **4c** (0.150 g, 0.224 mmol). Yield = 0.159 g, 81% of orange solid (R_f = 0.18). M.p. 75–77 °C. ^{1}H NMR ($CDCl_3$): δ 4.20 (s, 15H, C_5H_5), 4.19 (s, 6H, β-C_5H_4R), 4.18 (s, 6H, α-C_5H_4R), 2.61 (m, 6H, $C_5H_4CH_2$), 2.06 (m, 6H, CH_2P). $^{13}C\{^1H\}$ NMR ($CDCl_3$): δ 209.4 (d, $^2J_{CP}$ = 21 Hz, *cis*-CO), 206.3 (d, $^2J_{CP}$ = 9 Hz, *trans*-CO), 88.0 (d, $^3J_{CP}$ = 15 Hz, *ipso*-C_5H_4R), 68.6 (s, C_5H_5), 67.8 (s, α-C_5H_4R), 67.6 (s, β-C_5H_4R), 31.1 (d, $^1J_{CP}$ = 18 Hz, CH_2P), 24.3 (s, $C_5H_4CH_2$). ^{31}P NMR ($CDCl_3$): δ 12.5 (m). FT-IR: 3094 (w), 2928 (w), 2067 (m), 1981 (w), 1929 (s), 1634 (w), 1411 (w), 1106 (w), 1000 (w), 818 (w), 610 (m) cm^{-1}. UV-Vis (CH_2Cl_2): λ_{max} 435 nm (ε = 350 M^{-1} cm^{-1}). Mass Spec. (EI, +ve mode): exact mass calculated for $[C_{41}H_{39}{}^{56}Fe_3{}^{98}MoO_5P]^+$: 907.9637; exact mass found: 907.9595; difference: –4.6 ppm. Anal. Calcd. (%) for $C_{41}H_{39}Fe_3MoO_5P$: C, 54.34; H, 4.34. Found: C, 54.40; H, 4.38.

Primary phosphine complex 7a (M = W)

From $W(CO)_6$ (0.428 g, 1.22 mmol, 5 equiv.) and phosphine **4a** (0.060 g, 0.244 mmol). Yield = 0.124 g, 89% of orange solid (R_f = 0.35). M.p. 74–76 °C. ^{1}H NMR ($CDCl_3$): δ 4.55 (d of m, $^1J_{HP}$ = 332 Hz, 2H, PH_2), 4.14 (s, 5H, C_5H_5), 4.13 (*pseudo*-t, $^3J_{HH}$ = 2 Hz, 2H, β-C_5H_4R), 4.11 (*pseudo*-t, $^3J_{HH}$ = 2 Hz, 2H, α-C_5H_4R), 2.70 (m, 2H, $C_5H_4CH_2$), 2.12 (m, 2H, CH_2PH_2). $^{13}C\{^1H\}$ NMR ($CDCl_3$): δ 198.1 (d, $^2J_{CP}$ = 22 Hz, *cis*-CO), 195.5 (d, $^2J_{CP}$ = 7 Hz, *trans*-CO), 86.6 (d, $^3J_{CP}$ = 12 Hz, *ipso*-C_5H_4R), 68.7 (s, C_5H_5), 68.1 (s, α-C_5H_4R), 67.8 (s, β-C_5H_4R), 30.5 (d, $^2J_{CP}$ = 5 Hz, $C_5H_4CH_2$), 23.9 (d, $^1J_{CP}$ = 28 Hz, CH_2PH_2). ^{31}P NMR ($CDCl_3$): δ –101.9 (t of m, 86%, $^1J_{PH}$ = 333 Hz), –101.9 (t of d of m, 14%, $^1J_{PH}$ = 333 Hz, $^1J_{PW}$ = 217 Hz). FT-IR: 3092 (w), 2917 (w), 2345 (w), 2074 (m), 1976 (w),

Please do not adjust margins

Please do not adjust margins

1912 (s), 1638 (w), 1439 (w), 1411 (w), 1318 (w), 1105 (w), 1089 (w), 1000 (w), 926 (w), 884 (w), 821 (w), 676 (w) cm^{-1}. UV-Vis (CH_2Cl_2): λ_{max} 441 nm (ε = 120 M^{-1} cm^{-1}). Mass Spec. (EI, +ve mode): exact mass calculated for $[C_{17}H_{15}{}^{56}FeO_5P^{184}W]^+$: 569.9516; exact mass found: 569.9517; difference: +0.2 ppm. Anal. Calcd. (%) for $C_{17}H_{15}FeO_5PW$: C, 35.82; H, 2.65. Found: C, 36.06; H, 2.55.

Secondary phosphine complex 7b (M = W)

From $W(CO)_6$ (0.384 g, 1.09 mmol, 5 equiv.) and phosphine **4b** (0.100 g, 0.218 mmol). Yield = 0.154 g, 90% of orange solid (R_f = 0.22). M.p. 84–86 °C. ^{1}H NMR ($CDCl_3$): δ 4.85 (d of m, $^1J_{HP}$ = 327 Hz, 1H, P*H*), 4.14 (s, 10H, C_5H_5), 4.12 (*pseudo*-t, $^3J_{HH}$ = 2 Hz, 8H, *α*-C_5H_4R and *β*-C_5H_4R), 2.62 (m, 4H, $C_5H_4CH_2$), 2.16 (m, 4H, CH_2PH). $^{13}C\{^1H\}$ NMR ($CDCl_3$): δ 198.7 (d, $^2J_{CP}$ = 21 Hz, *cis*-*C*O), 196.4 (d, $^2J_{CP}$ = 7 Hz, *trans*-*C*O), 87.3 (d, $^3J_{CP}$ = 14 Hz, *ipso*-C_5H_4R), 68.7 (s, C_5H_5), 67.8 (d, $^4J_{CP}$ = 17 Hz, *α*-C_5H_4R), 67.7 (s, *β*-C_5H_4R), 28.1 (d, $^1J_{CP}$ = 25 Hz, CH_2PH), 27.1 (s, $C_5H_4CH_2$). ^{31}P NMR ($CDCl_3$): δ –43.6 (d of m, 86%, $^1J_{PH}$ = 328 Hz), –43.6 (d of d of m, 14%, $^1J_{PH}$ = 328 Hz, $^1J_{PW}$ = 225 Hz). FT-IR: 3092 (w), 2917 (w), 2070 (m), 1978 (w), 1914 (s), 1640 (w), 1411 (w), 1219 (w), 1105 (w), 1000 (w), 820 (w), 772 (s), 599 (w) cm^{-1}. UV-Vis (CH_2Cl_2): λ_{max} 437 nm (ε = 245 M^{-1} cm^{-1}). Mass Spec. (EI, +ve mode): exact mass calculated for $[C_{29}H_{27}{}^{56}Fe_2O_5P^{184}W]^+$: 781.9804; exact mass found: 781.9791; difference: –1.7 ppm. Anal. Calcd. (%) for $C_{29}H_{27}Fe_2O_5PW$: C, 44.54; H, 3.48. Found: C, 44.70; H, 3.44.

Tertiary phosphine complex 7c (M = W)

From $W(CO)_6$ (0.394 g, 1.12 mmol, 5 equiv.) and phosphine **4c** (0.150 g, 0.224 mmol). Yield = 0.194 g, 87% of orange solid (R_f = 0.18). M.p. 143–145 °C. ^{1}H NMR ($CDCl_3$): δ 4.15 (s, 15H, C_5H_5), 4.14 (s, 12H, *α*-C_5H_4R and *β*-C_5H_4R), 2.56 (m, 6H, $C_5H_4CH_2$), 2.11 (m, 6H, CH_2P). $^{13}C\{^1H\}$ NMR ($CDCl_3$): δ 198.8 (d, $^2J_{CP}$ = 21 Hz, *cis*-*C*O), 197.2 (d, $^2J_{CP}$ = 8 Hz, *trans*-*C*O), 87.8 (d, $^3J_{CP}$ = 15 Hz, *ipso*-C_5H_4R), 68.6 (s, C_5H_5), 67.8 (s, *α*-C_5H_4R), 67.6 (s, *β*-C_5H_4R), 31.6 (d, $^1J_{CP}$ = 22 Hz, CH_2P), 24.6 (s, $C_5H_4CH_2$). ^{31}P NMR ($CDCl_3$): δ –6.8 (m, 86%), –6.8 (d of m, 14%, $^1J_{PW}$ = 233 Hz). FT-IR: 3090 (w), 2924 (w), 2066 (m), 1974 (w), 1922 (s), 1635 (w), 1411 (w), 1415 (w), 1442 (w), 1321 (w), 1230 (w), 1105 (w), 1000 (w), 820 (w), 754 (w), 601 (w) cm^{-1}. UV-Vis (CH_2Cl_2): λ_{max} 436 nm (ε = 335 M^{-1} cm^{-1}). Mass Spec. (EI, +ve mode): exact mass calculated for $[C_{41}H_{39}{}^{56}Fe_3O_5P^{184}W]^+$: 994.0093; exact mass found: 994.0095; difference: +0.2 ppm. Anal. Calcd. (%) for $C_{41}H_{39}Fe_3O_5PW$: C, 49.54; H, 3.95. Found: C, 50.07; H, 4.03.

Acknowledgements

We would like to thank the University of Western Ontario, the Natural Science and Engineering Research Council (NSERC) of Canada (P.J.R., J.B.G.: DG, 311921, 435675), and the Ontario Ministry of Research and Innovation (J.B.G.: ERA, ER14-10-147) for funding this work. We also thank Cytec Canada Inc. for providing phosphine gas and expertise surrounding its safe usage. Finally, we acknowledge Dr. Paul D. Boyle and Stephanie M. Barbon for X-ray crystallography.

Notes and references

1 Selected examples: (a) B. L. Ghent, L. A. Sites, A. L. Rheingold and C. Nataro, *Organometallics*, 2005, **24**, 4788–4792; (b) R. Kalio, P. Lönnecke and E. Hey-Hawkins, *J. Organomet. Chem.*, 2008, **693**, 590–600; (c) C.-G. Chen, X.-L. Hou and L. Pu, *Org. Lett.*, 2009, **11**, 2073–2075; (d) A. Zirakzadeh, R. Schuecker, N. Gorgas, K. Mereiter, F. Spindler and W. Weissensteiner, *Organometallics*, 2012, **31**, 4241–4250; (e) C. B. Khadka, B. K. Najafabadi, M. Hesari, M. S. Workentin and J. F. Corrigan, *Inorg. Chem.*, 2013, **52**, 6798–6805; (f) B. E. Cowie, F. A. Tsao and D. J. H. Emslie, *Angew. Chem. Int. Ed.*, 2015, **54**, 2165–2169.

2 Selected books and reviews: (a) G. Erre, S. Enthaler, K. Junge, S. Gladiali and M. Beller, *Coord. Chem. Rev.*, 2008, **252**, 471–491; (b) K. H. Shaughnessy, *Chem. Rev.*, 2009, **109**, 643–710; (c) *Phosphorus(III) Ligands in Homogeneous Catalysis: Design and Synthesis*, Wiley-Blackwell, Oxford, 2012; (d) S. H. Chikkali, J. I. van der Vlugt and J. N. H. Reek, *Coord. Chem. Rev.*, 2014, **262**, 1–15; (e) B. P. Nell and D. R. Tyler, *Coord. Chem. Rev.*, 2014, **279**, 23–42.

3 Selected examples: (a) S. P. Annen, V. Bambagioni, M. Bevilacqua, J. Filippi, A. Marchionni, W. Oberhauser, H. Schönberg, F. Vizza, C. Bianchini and H. Grützmacher, *Angew. Chem. Int. Ed.*, 2010, **49**, 7229–7233; (b) J. S. Anderson, J. Rittle and J. C. Peters, *Nature*, 2013, **501**, 84–87; (c) P. Kang, S. Zhang, T. J. Meyer and M. Brookhart, *Angew. Chem. Int. Ed.*, 2014, **53**, 8709–8713; (d) K. T. Horak, A. Velian, M. W. Day and T. Agapie, *Chem. Commun.*, 2014, **50**, 4427–4429; (e) B. J. Johnson, S. V. Lindeman and N. P. Mankad, *Inorg. Chem.*, 2014, **53**, 10611–10619; (f) H. Tinnermann, C. Wille and M. Alcarazo, *Angew. Chem. Int. Ed.*, 2014, **53**, 8732–8736; (g) X. Yan, T. R. Cook, P. Wang, F. Huang and P. J. Stang, *Nat. Chem.*, 2015, **7**, 342–348; (h) D. Zhao, T. M. Neubauer and B. L. Feringa, *Nat. Commun.*, 2015, **6**; (i) E. L. Hazeland, A. M. Chapman, P. G. Pringle and H. A. Sparkes, *Chem. Commun.*, 2015, **51**, 10206–10209.

4 C. A. Tolman, *Chem. Rev.*, 1977, **77**, 313–348.

5 M. L. Clarke and J. J. R. Frew, in *Organometallic Chemistry: Volume 35*, eds. I. J. S. Fairlamb and J. M. Lynam, The Royal Society of Chemistry, Cambridge, 2009, pp. 19–46.

6 Selected examples: (a) A. Staubitz, A. P. Soto and I. Manners, *Angew. Chem. Int. Ed.*, 2008, **47**, 6212–6215; (b) E. Piedra-Arroni, C. Ladavière, A. Amgoune and D. Bourissou, *J. Am. Chem. Soc.*, 2013, **135**, 13306–13309; (c) A. Nakamura, T. M. J. Anselment, J. Claverie, B. Goodall, R. F. Jordan, S. Mecking, B. Rieger, A. Sen, P. W. N. M. van Leeuwen and K. Nozaki, *Acc. Chem. Res.*, 2013, **46**, 1438–1449; (d) H.-K. Lee, K.-T. Bang, A. Hess, R. H. Grubbs and T.-L. Choi, *J. Am. Chem. Soc.*, 2015, **137**, 9262–9265; (e) E. Bultz, M. Ouchi, K. Nishizawa, M. F. Cunningham and M. Sawamoto, *ACS Macro Lett.*, 2015, **4**, 628–631.

7 Selected examples: (a) G. E. Dobereiner, J. Yuan, R. R. Schrock, A. S. Goldman and J. D. Hackenberg, *J. Am. Chem. Soc.*, 2013, **135**, 12572–12575; (b) C. Cheng and J. F. Hartwig, *J. Am. Chem. Soc.*, 2014, **136**, 12064–12072; (c) A. Borzenko, N. L. Rotta-Loria, P. M. MacQueen, C. M. Lavoie, R. McDonald and M. Stradiotto, *Angew. Chem. Int. Ed.*, 2015, **54**, 3773–3777; (d) E. J. Tollefson, L. E. Hanna and E. R. Jarvo, *Acc. Chem. Res.*, 2015, **48**, 2344–2353; (e) Y. Yang, S.-L. Shi, D. Niu, P. Liu and S. L. Buchwald, *Science*, 2015, **349**, 62–66; (f) S. A. Tymonko, R. C. Smith, A. Ambrosi, M. H. Ober, H. Wang and S. E. Denmark, *J. Am. Chem. Soc.*, 2015, **137**, 6200–6218.

This journal is © The Royal Society of Chemistry 20xx

Please do not adjust margins

Please do not adjust margins

8 Selected examples: (a) M. R. Friedfeld, G. W. Margulieux, B. A. Schaefer and P. J. Chirik, *J. Am. Chem. Soc.*, 2014, **136**, 13178–13181; (b) T. Zell, Y. Ben-David and D. Milstein, *Angew. Chem. Int. Ed.*, 2014, **53**, 4685-4689; (c) A. Zirakzadeh, M. A. Groß, Y. Wang, K. Mereiter and W. Weissensteiner, *Organometallics*, 2014, **33**, 1945–1952; (d) C. Guo, D.-W. Sun, S. Yang, S.-J. Mao, X.-H. Xu, S.-F. Zhu and Q.-L. Zhou, *J. Am. Chem. Soc.*, 2015, **137**, 90–93; (e) S. Wesselbaum, V. Moha, M. Meuresch, S. Brosinski, K. M. Thenert, J. Kothe, T. vom Stein, U. Englert, M. Hölscher, J. Klankermayer and W. Leitner, *Chem. Sci.*, 2015, **6**, 693–704; (f) W. Zuo and R. H. Morris, *Nat. Protoc.*, 2015, **10**, 241–257.

9 Selected Reviews: (a) M. Brynda, *Coord. Chem. Rev.*, 2005, **249**, 2013–2034; (b) J. T. Fleming and L. J. Higham, *Coord. Chem. Rev.*, 2015, **297–298**, 127–145.

10 Selected examples: (a) G. Ramakrishnan, A. Jouaiti, M. Geoffroy and G. Bernardinelli, *J. Phys. Chem.*, 1996, **100**, 10861–10868; (b) K. R. Prabhu, N. Pillarsetty, H. Gali and K. V. Katti, *J. Am. Chem. Soc.*, 2000, **122**, 1554–1555; (c) W. Henderson and S. R. Alley, *J. Organomet. Chem.*, 2002, **656**, 120–128; (d) R. M. Hiney, L. J. Higham, H. Müller-Bunz and D. G. Gilheany, *Angew. Chem. Int. Ed.*, 2006, **45**, 7248–7251; (e) T. E. Barder and S. L. Buchwald, *J. Am. Chem. Soc.*, 2007, **129**, 5096–5101; (f) B. Stewart, A. Harriman and L. J. Higham, *Organometallics*, 2011, **30**, 5338–5343; (g) L. H. Davies, B. Stewart, R. W. Harrington, W. Clegg and L. J. Higham, *Angew. Chem. Int. Ed.*, 2012, **51**, 4921–4924; (h) T. Asamizu, W. Henderson, B. K. Nicholson and E. Hey-Hawkins, *Inorg. Chim. Acta*, 2014, **414**, 181–190.

11 (a) A. Rabiee Kenaree, B. M. Berven, P. J. Ragogna and J. B. Gilroy, *Chem. Commun.*, 2014, **50**, 10714–10717; (b) A. Rabiee Kenaree, T. J. Cuthbert, S. M. Barbon, P. D. Boyle, E. R. Gillies, P. J. Ragogna and J. B. Gilroy, *Organometallics*, 2015, **34**, 4272–4280.

12 R. Guterman, A. Rabiee Kenaree, J. B. Gilroy, E. R. Gillies and P. J. Ragogna, *Chem. Mater.*, 2015, **27**, 1412–1419.

13 R. Guterman, E. R. Gillies and P. J. Ragogna, *Dalton Trans.*, 2015, **44**, 15664–15670.

14 Selected examples: (a) A. Labande, J. Ruiz and D. Astruc, *J. Am. Chem. Soc.*, 2002, **124**, 1782–1789; (b) R. L. Stiles, R. Balasubramanian, S. W. Feldberg and R. W. Murray, *J. Am. Chem. Soc.*, 2008, **130**, 1856–1865; (c) K. A. Mahmoud, S. Hrapovic and J. H. T. Luong, *ACS Nano*, 2008, **2**, 1051–1057; (d) R. C. Mulrooney, N. Singh, N. Kaur and J. F. Callan, *Chem. Commun.*, 2009, 686-688; (e) M. Aminur Rahman, J. Ik Son, M.-S. Won and Y.-B. Shim, *Anal. Chem.*, 2009, **81**, 6604–6611; (f) Y. Liu, B. Khalili Najafabadi, M. Azizpoor Fard and J. F. Corrigan, *Angew. Chem. Int. Ed.*, 2015, **54**, 4832–4835.

15 S. O. Grim, P. R. McAllister and R. M. Singer, *Chem. Commun.*, 1969, 38–39.

16 (a) L. E. Orgel, *Inorg. Chem.*, 1962, **1**, 25–29; (b) F. A. Cotton and C. S. Kraihanzel, *J. Am. Chem. Soc.*, 1962, **84**, 4432–4438.

17 J. Dalton, I. Paul, J. G. Smith and F. G. A. Stone, *J. Chem. Soc. A*, 1968, 1195–1199.

18 Bruker-AXS, SAINT version 2013.8, 2013, Bruker-AXS, Madison, WI 53711, USA.

19 Bruker-AXS, SADABS version 2012.1, 2012, Bruker-AXS, Madison, WI 53711, USA.

20 Bruker-AXS, TWINABS version 2012.1, 2012, Bruker-AXS, Madison, WI 53711, USA.

21 GNU Octave https://www.gnu.org/software/octave/ version 3.6.4.

22 G. Sheldrick, *Acta Crystallogr.*, 2015, **A71**, 3–8.

23 G. Sheldrick, *Acta Crystallogr.*, 2008, **A64**, 112–122.

This journal is © The Royal Society of Chemistry 20xx

Please do not adjust margins

Supplementary Information

Group 6 Metal Pentacarbonyl Complexes of Air-Stable Primary, Secondary, and Tertiary Ferrocenylethylphosphines

*Amir Rabiee Kenaree, Ethan R. Sauvé, Paul J. Ragogna, Joe B. Gilroy**

Department of Chemistry and the Centre for Advanced Materials and Biomaterials Research (CAMBR), The University of Western Ontario, 1151 Richmond St. N., London, Ontario, Canada, N6A 5B7. Tel: +1-519-661-2111 ext. 81561, E-mail: joe.gilroy@uwo.ca.

Table of Contents

NMR Spectra.....S2

Solid-State Structures.....S18

FT-IR Absorption Spectra.....S19

UV-Vis Absorption Spectra.....S24

Cyclic Voltammograms.....S27

NMR Spectra

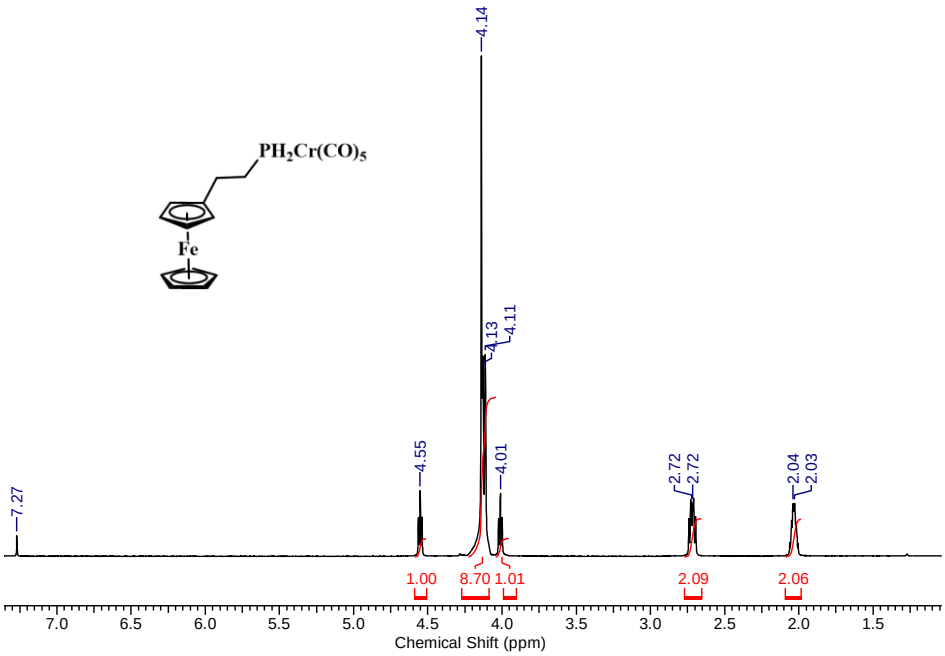

Fig. S1 ^{1}H NMR spectrum of **5a** in $CDCl_3$.

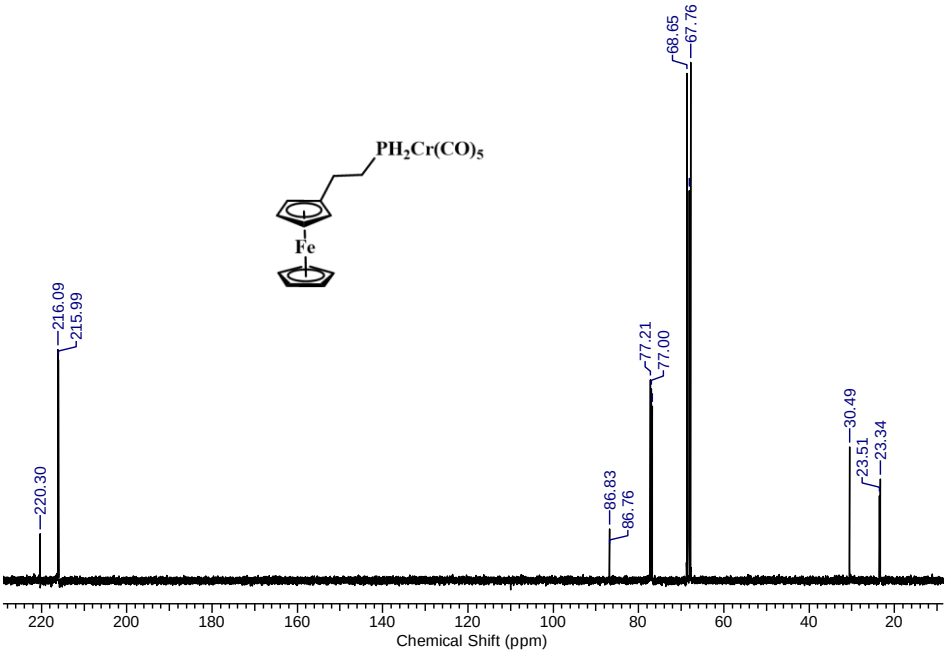

Fig. S2 ^{13}C{^{1}H} NMR spectrum of **5a** in $CDCl_3$.

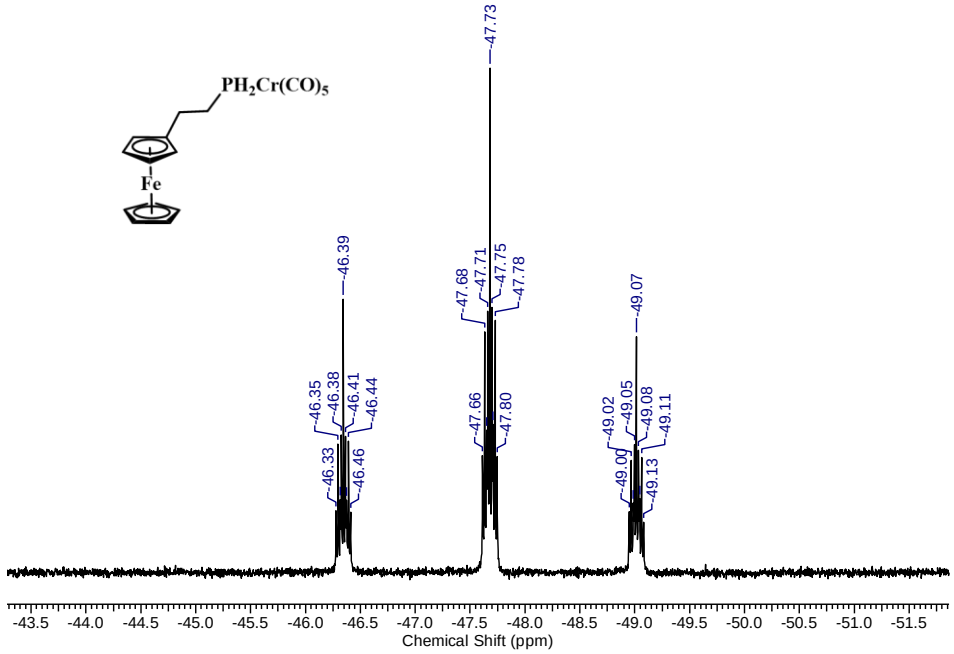

Fig. S3 ^{31}P NMR spectrum of **5a** in $CDCl_3$.

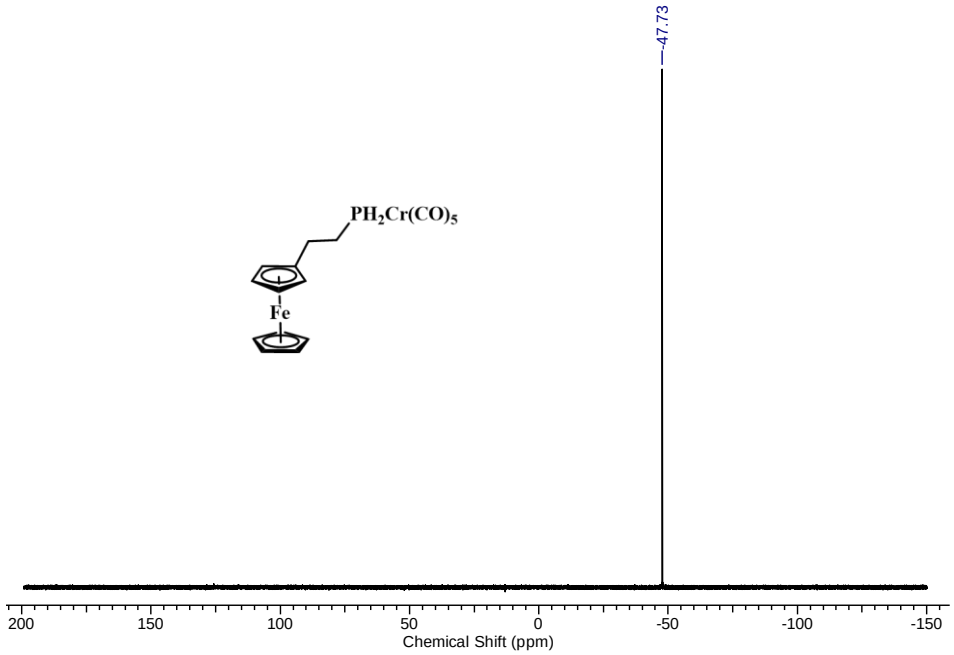

Fig. S4 $^{31}P\{^1H\}$ NMR spectrum of **5a** in $CDCl_3$.

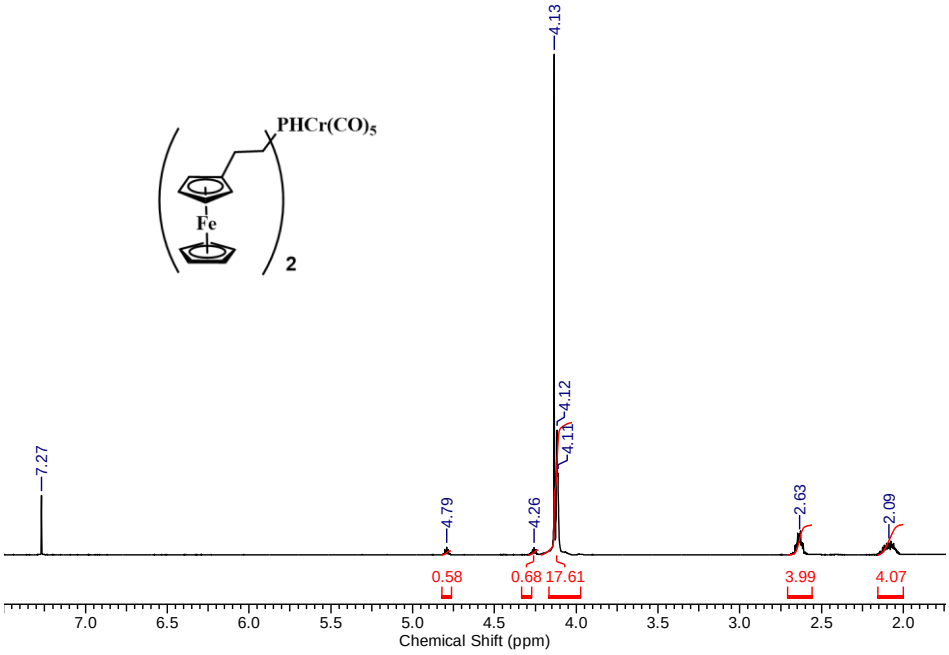

Fig. S5 ^{1}H NMR spectrum of **5b** in $CDCl_3$.

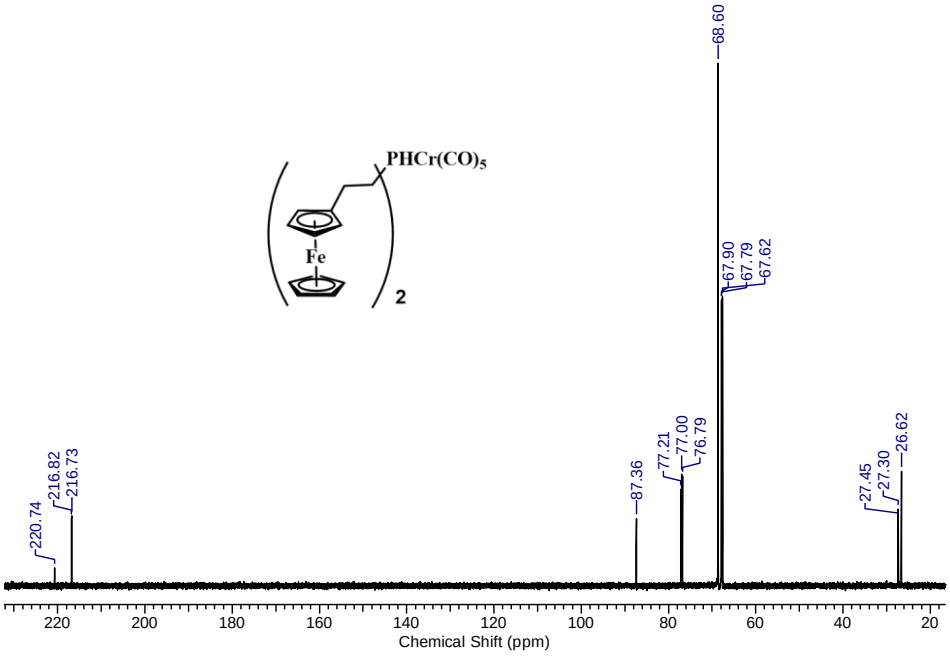

Fig. S6 ^{13}C{^{1}H} NMR spectrum of **5b** in $CDCl_3$.

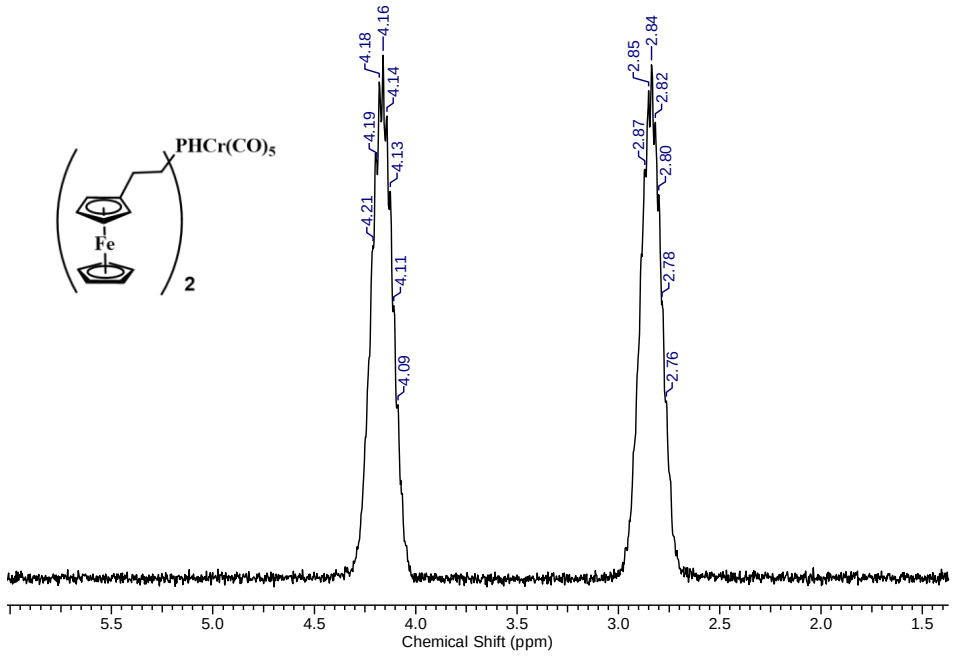

Fig. S7 ^{31}P NMR spectrum of **5b** in $CDCl_3$.

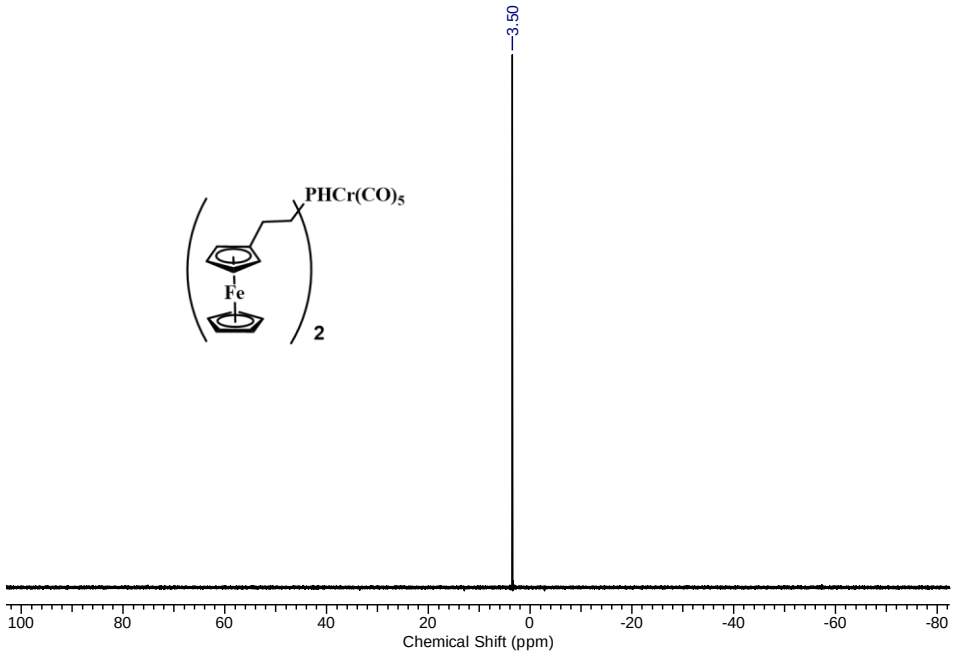

Fig. S8 $^{31}P\{^{1}H\}$ NMR spectrum of **5b** in $CDCl_3$.

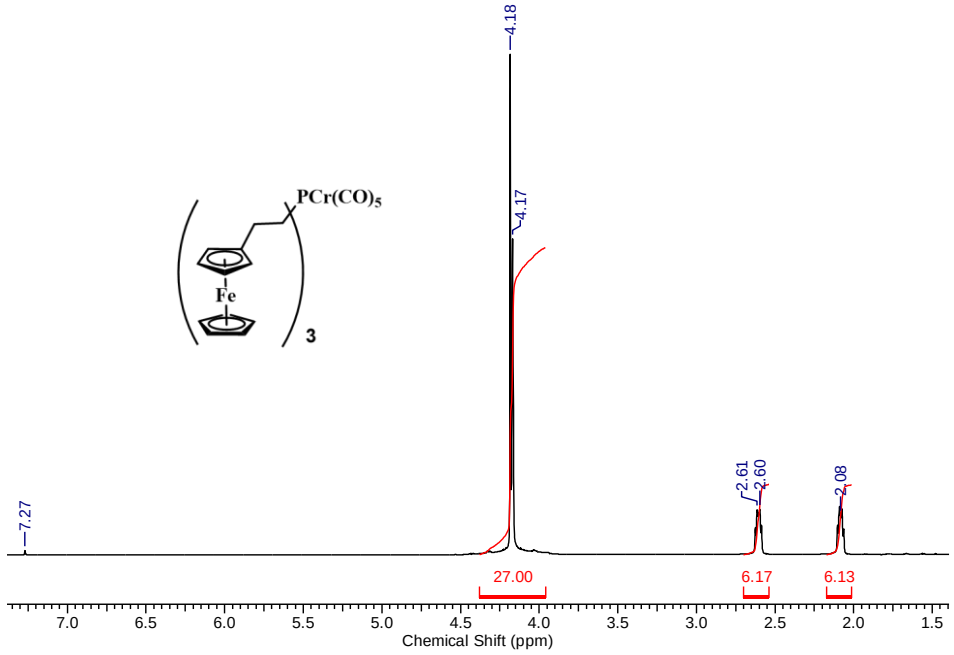

Fig. S9 ^{1}H NMR spectrum of **5c** in $CDCl_3$.

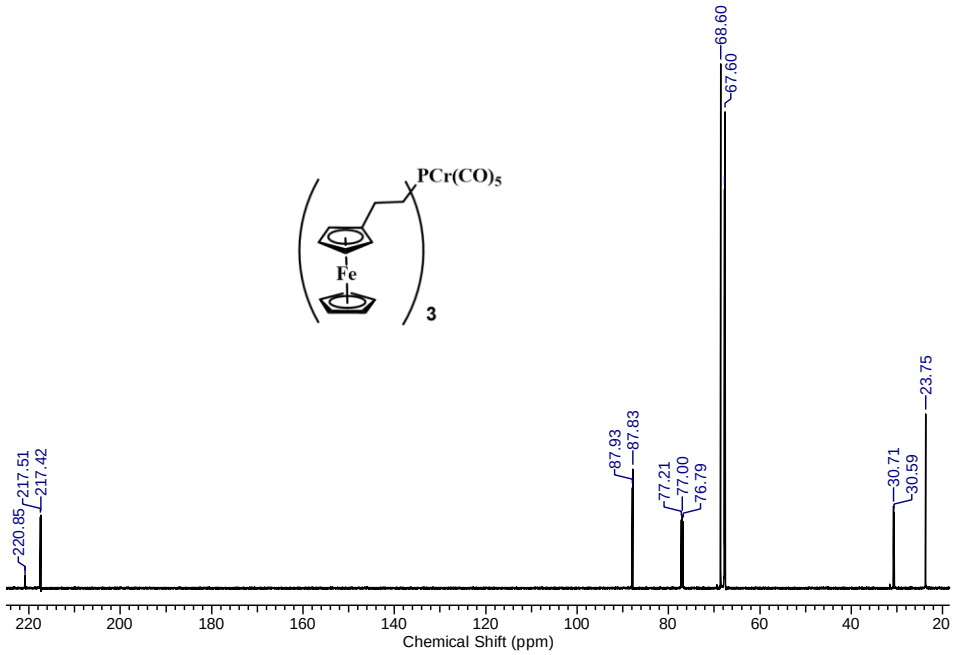

Fig. S10 ^{13}C{^{1}H} NMR spectrum of **5c** in $CDCl_3$.

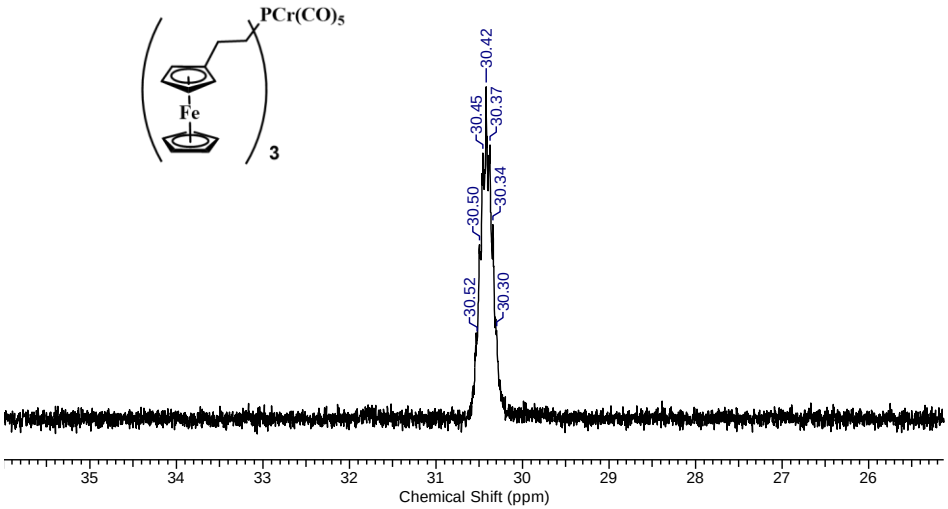

Fig. S11 ^{31}P NMR spectrum of **5c** in $CDCl_3$.

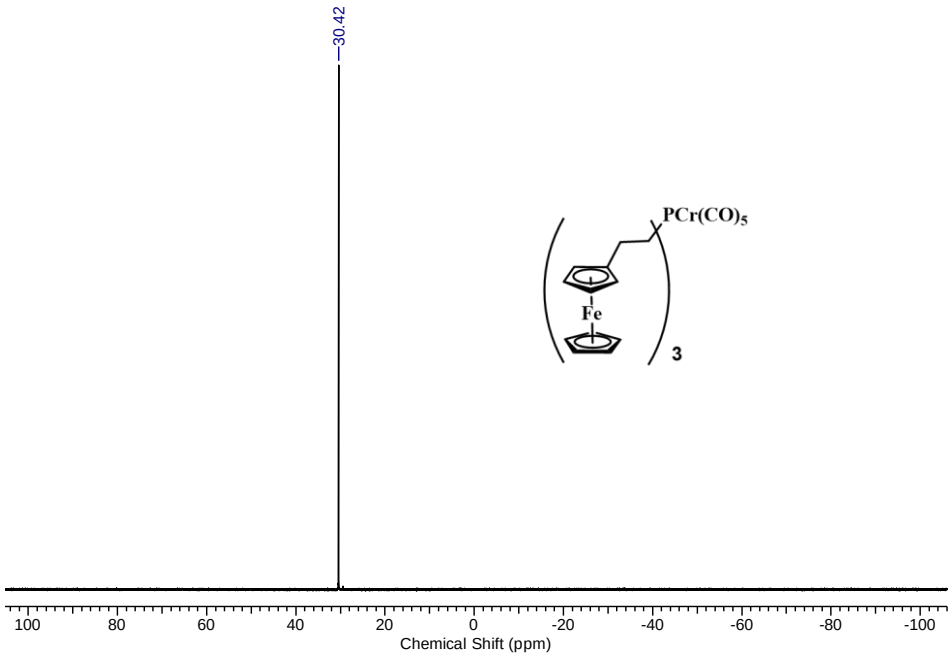

Fig. S12 $^{31}P\{^{1}H\}$ NMR spectrum of **5c** in $CDCl_3$.

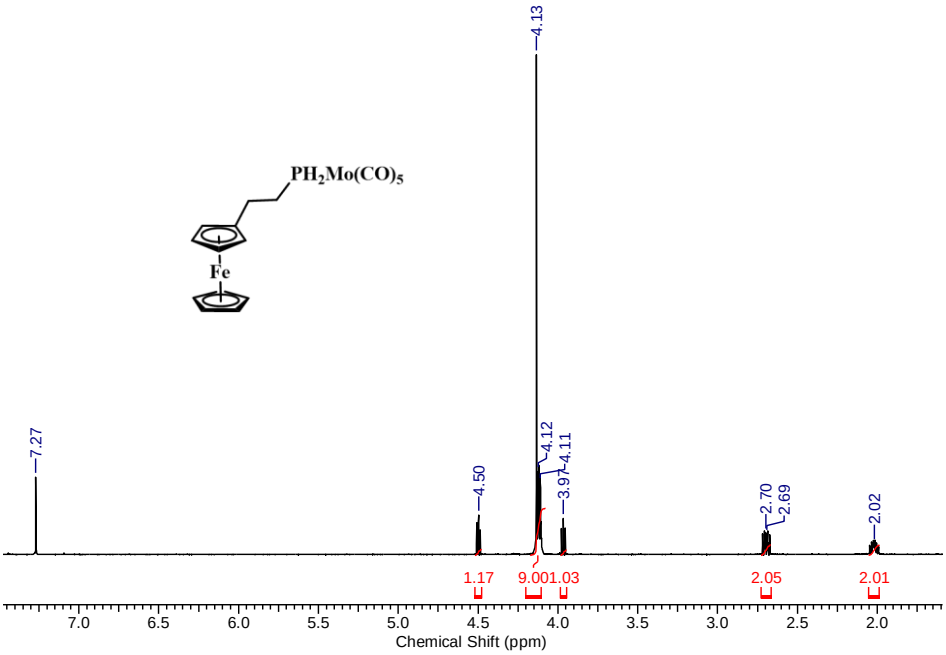

Fig. S13 ^{1}H NMR spectrum of **6a** in $CDCl_3$.

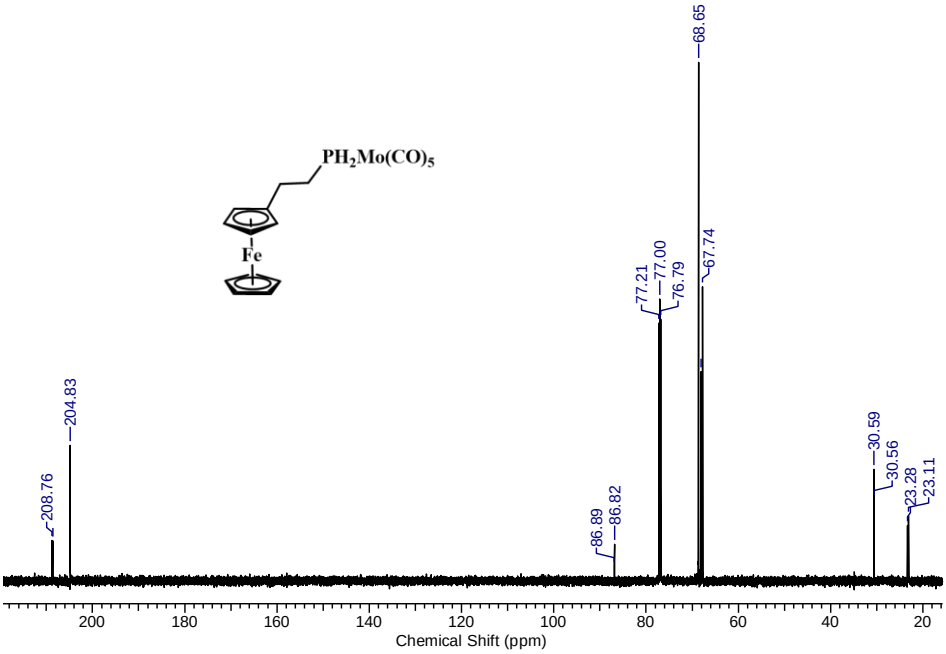

Fig. S14 ^{13}C{^{1}H} NMR spectrum of **6a** in $CDCl_3$.

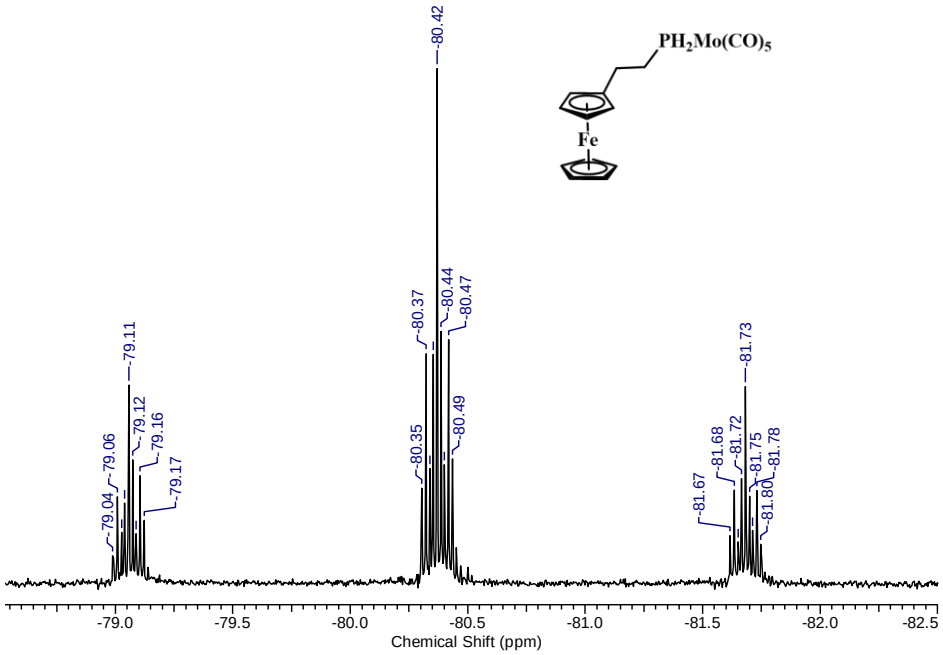

Fig. S15 ^{31}P NMR spectrum of **6a** in $CDCl_3$.

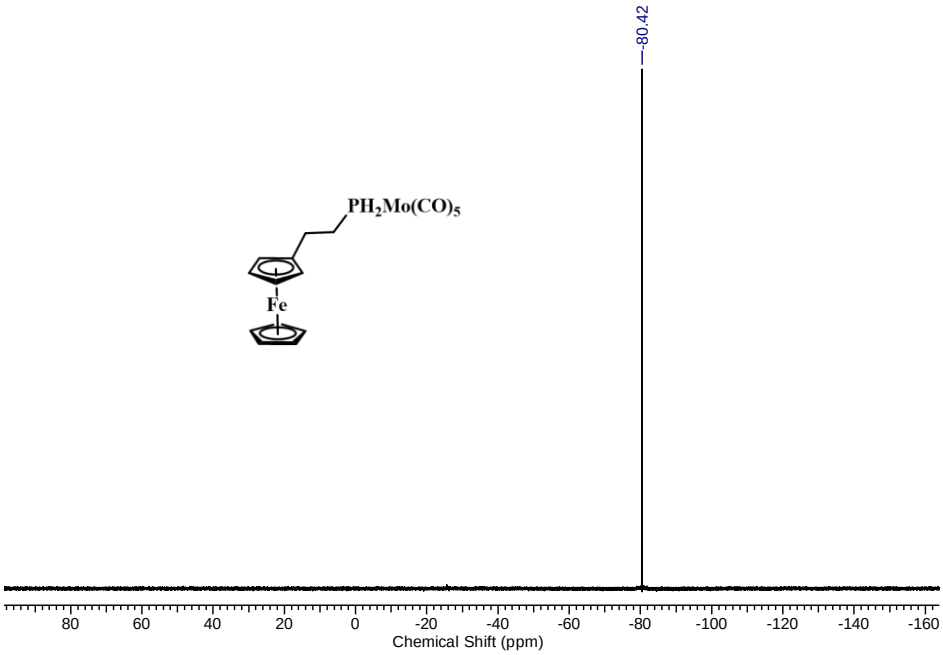

Fig. S16 $^{31}P\{^{1}H\}$ NMR spectrum of **6a** in $CDCl_3$.

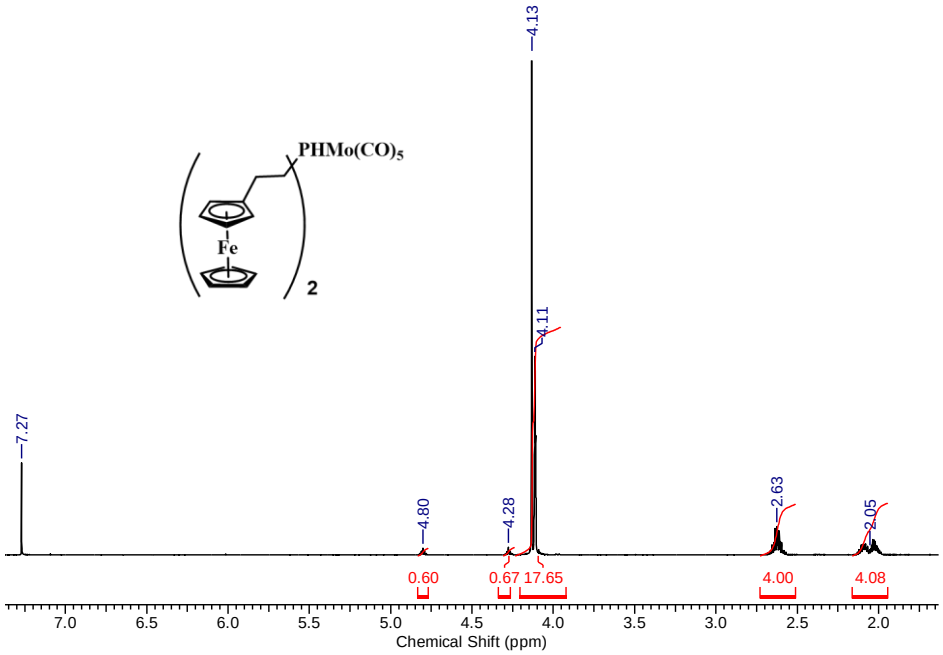

Fig. S17 ^{1}H NMR spectrum of **6b** in $CDCl_3$.

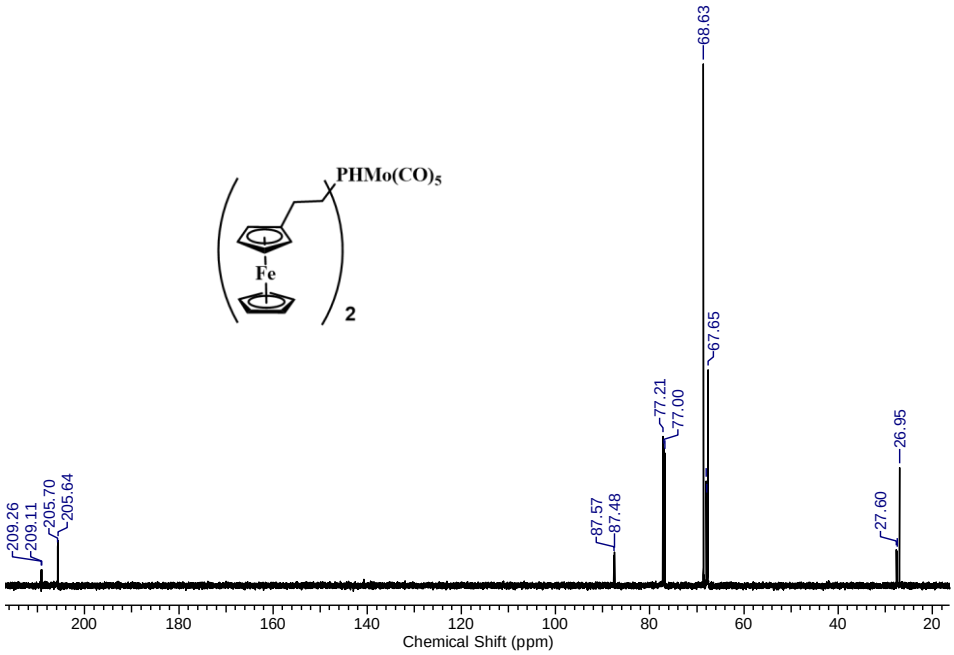

Fig. S18 ^{13}C{^{1}H} NMR spectrum of **6b** in $CDCl_3$.

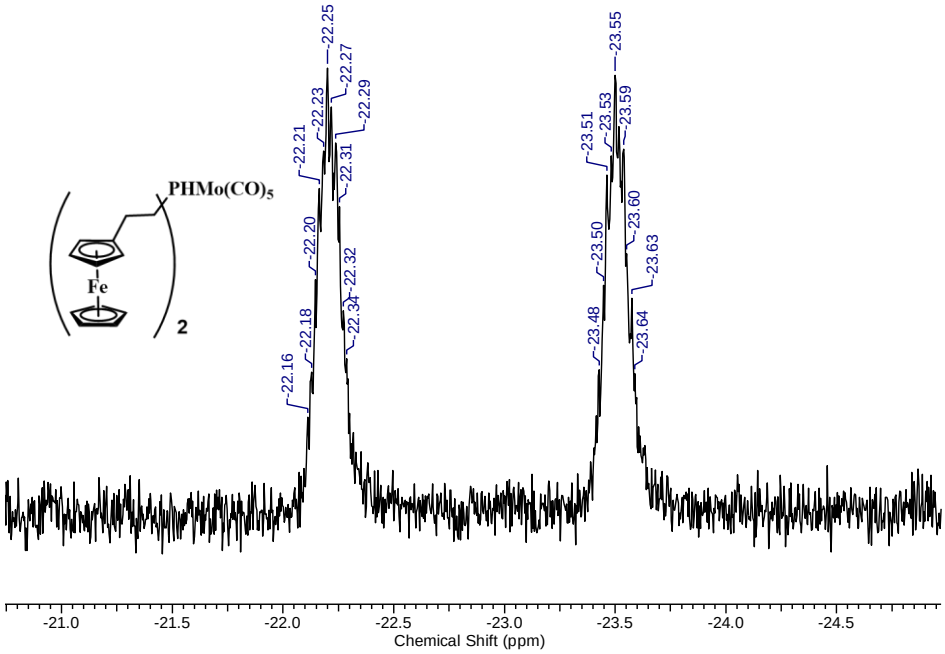

Fig. S19 ^{31}P NMR spectrum of **6b** in $CDCl_3$.

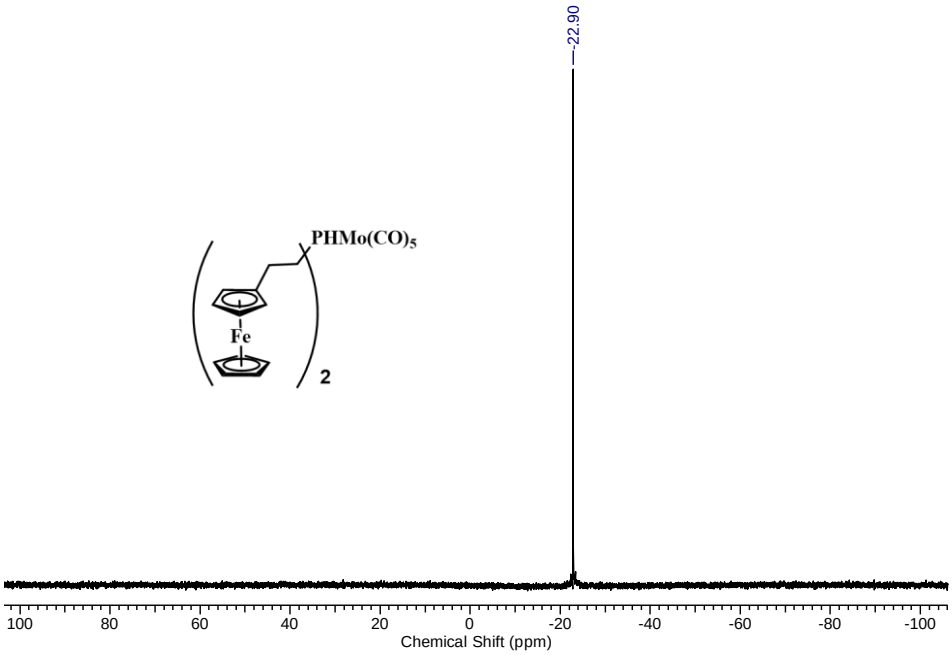

Fig. S20 $^{31}P\{^1H\}$ NMR spectrum of **6b** in $CDCl_3$.

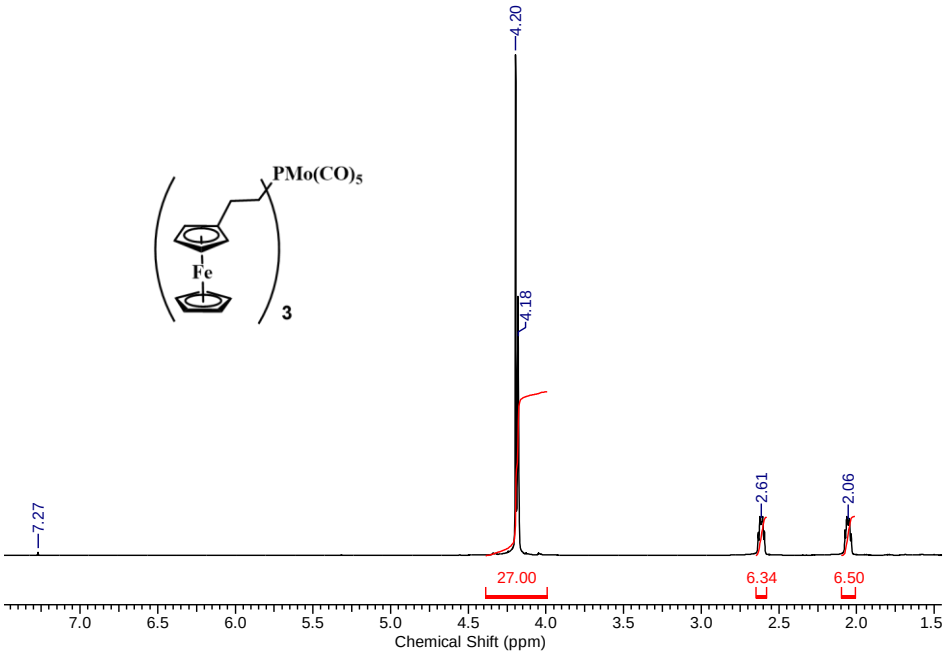

Fig. S21 ^{1}H NMR spectrum of **6c** in $CDCl_3$.

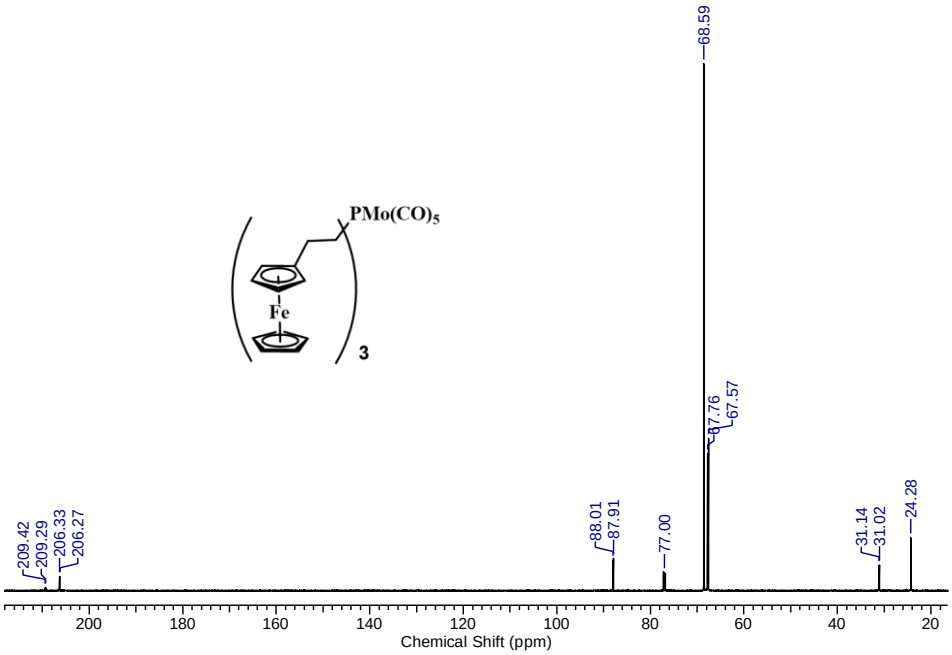

Fig. S22 ^{13}C{^{1}H} NMR spectrum of **6c** in $CDCl_3$.

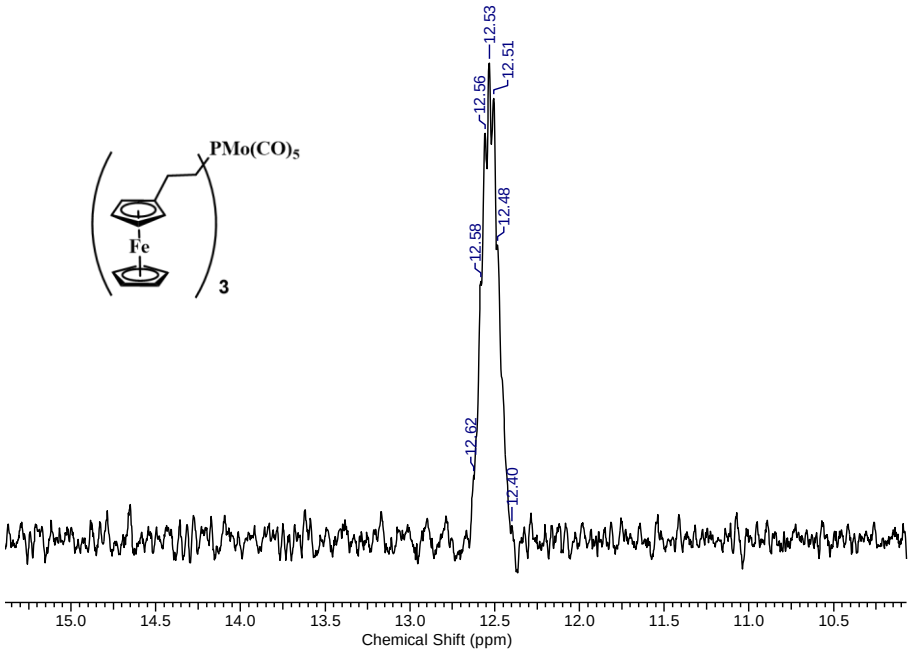

Fig. S23 ^{31}P NMR spectrum of **6c** in $CDCl_3$.

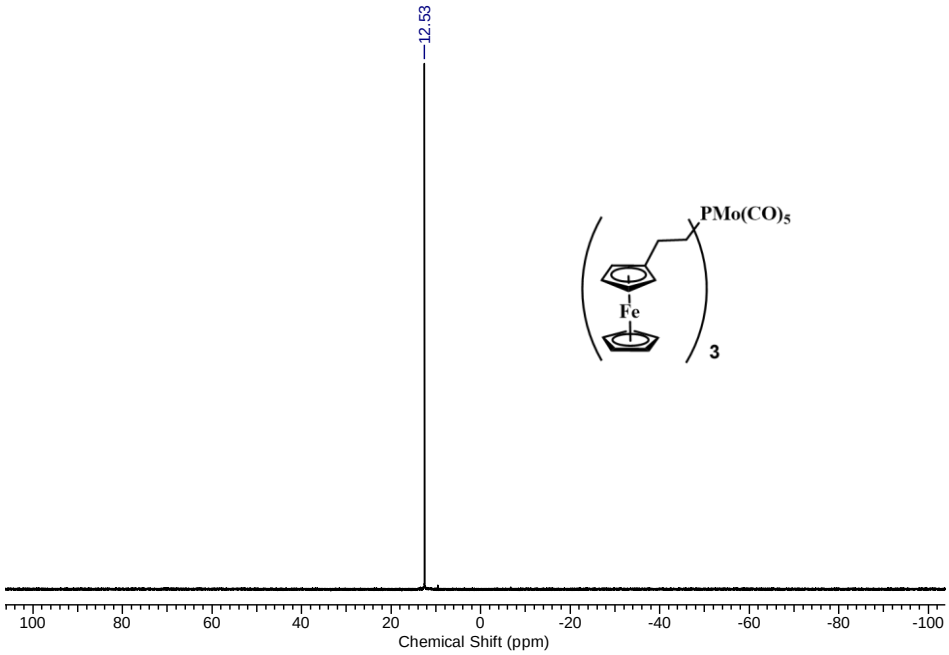

Fig. S24 $^{31}P\{^{1}H\}$ NMR spectrum of **6c** in $CDCl_3$.

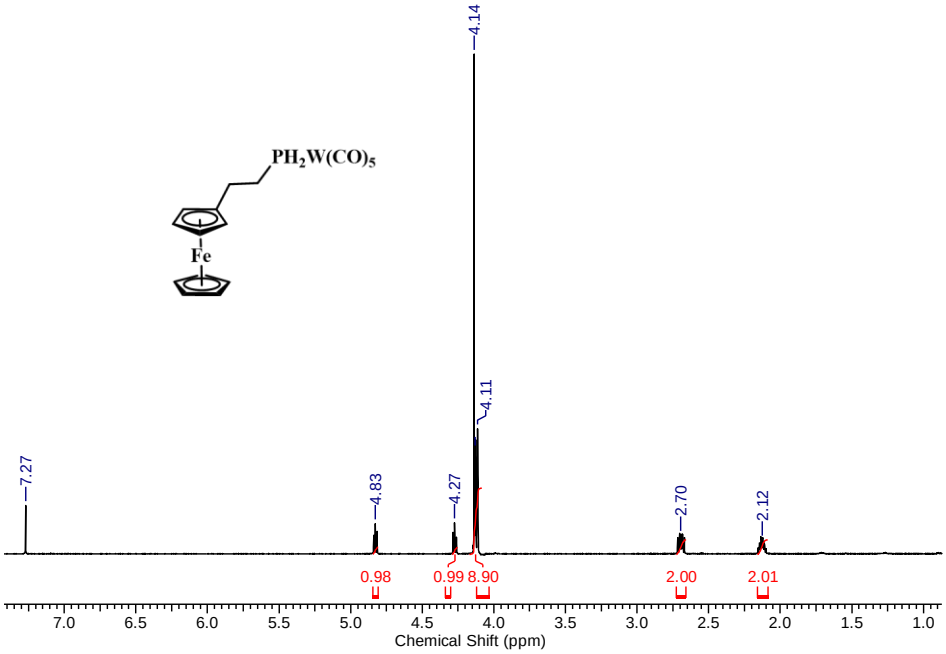

Fig. S25 ^{1}H NMR spectrum of **7a** in $CDCl_3$.

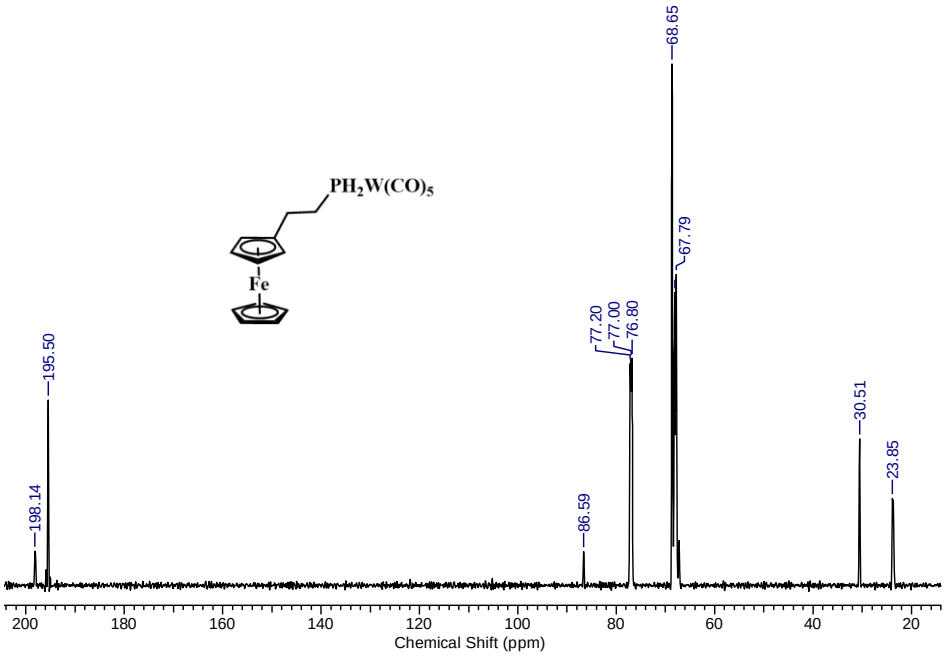

Fig. S26 ^{13}C{^{1}H} NMR spectrum of **7a** in $CDCl_3$.

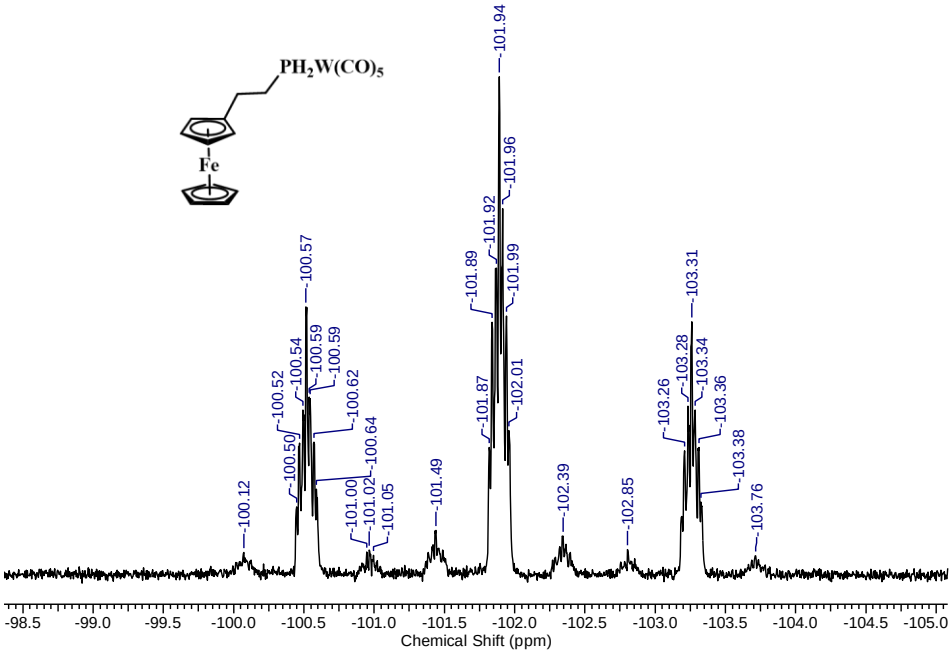

Fig. S27 ^{31}P NMR spectrum of **7a** in $CDCl_3$.

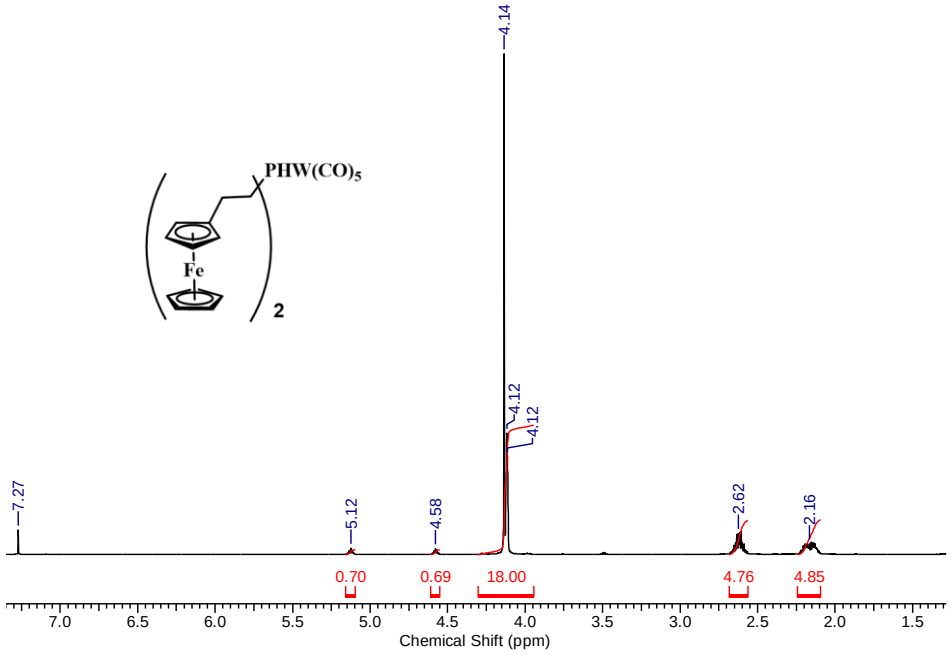

Fig. S28 ^{1}H NMR spectrum of **7b** in $CDCl_3$.

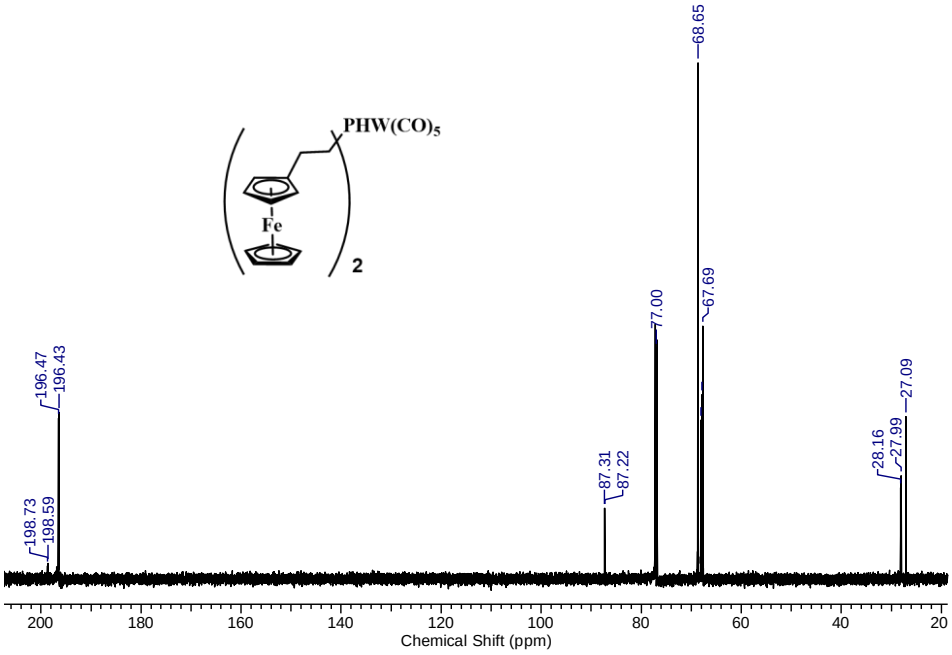

Fig. S29 $^{13}C\{^{1}H\}$ NMR spectrum of **7b** in $CDCl_3$.

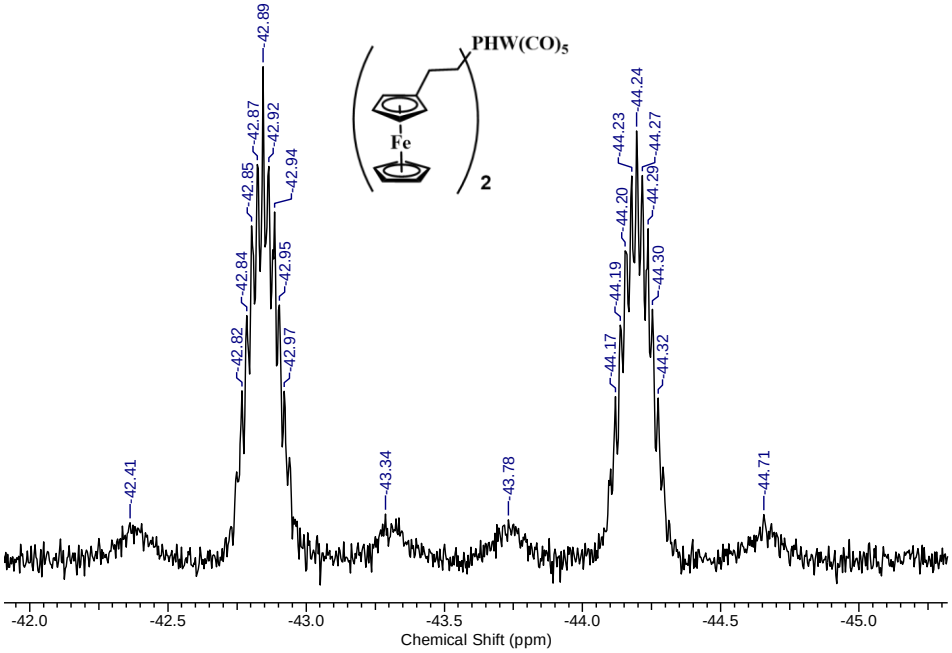

Fig. S30 ^{31}P NMR spectrum of **7b** in $CDCl_3$.

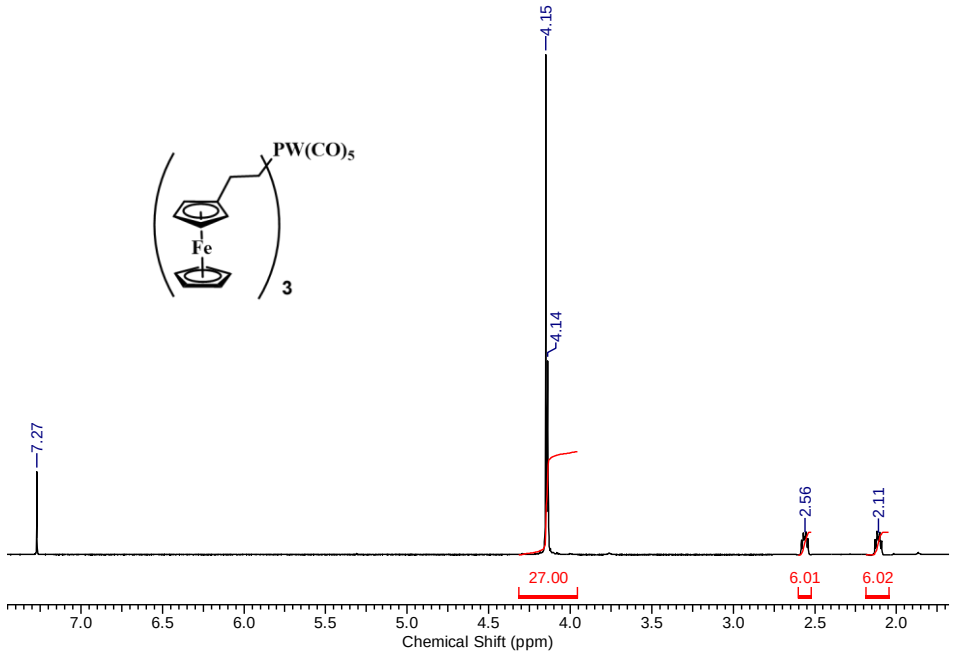

Fig. S31 ^{1}H NMR spectrum of **7c** in $CDCl_3$.

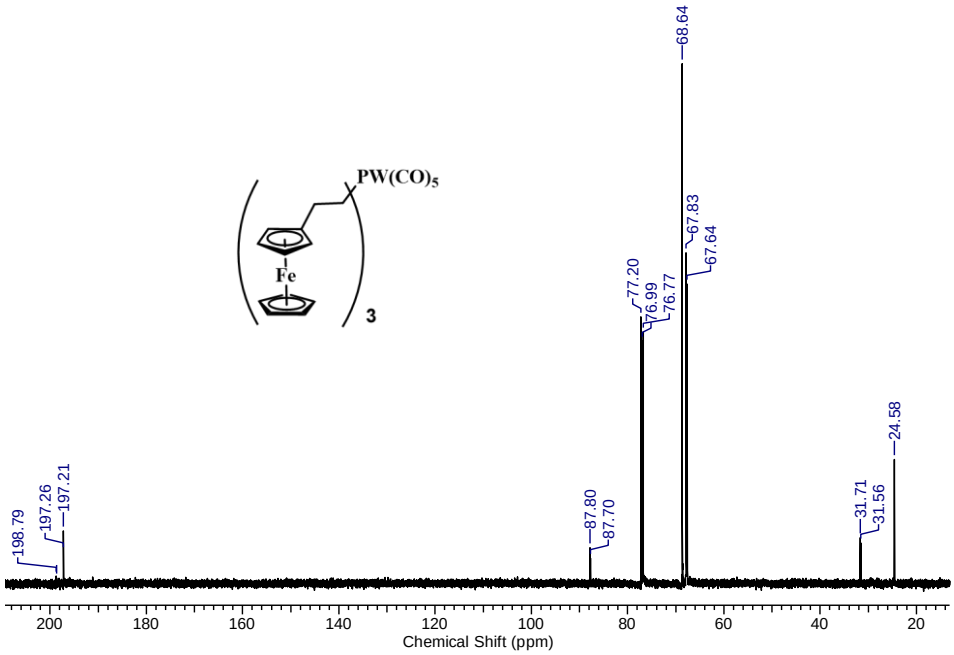

Fig. S32 $^{13}C\{^{1}H\}$ NMR spectrum of **7c** in $CDCl_3$.

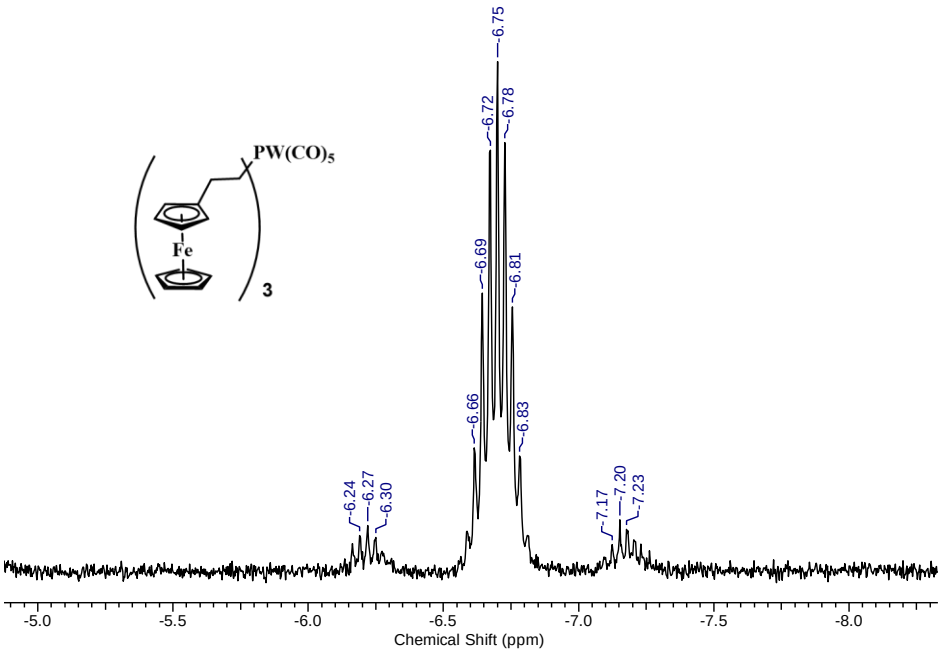

Fig. S33 ^{31}P NMR spectrum of **7c** in $CDCl_3$.

Solid-state structures

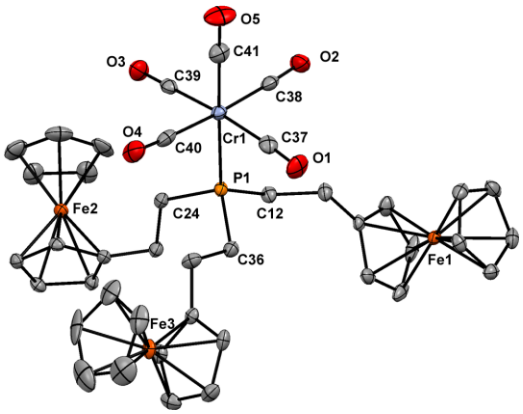

Fig. S34 Solid-state structure of **5c**. Anisotropic displacement ellipsoids are shown at 50% probability and hydrogen atoms have been omitted for clarity.

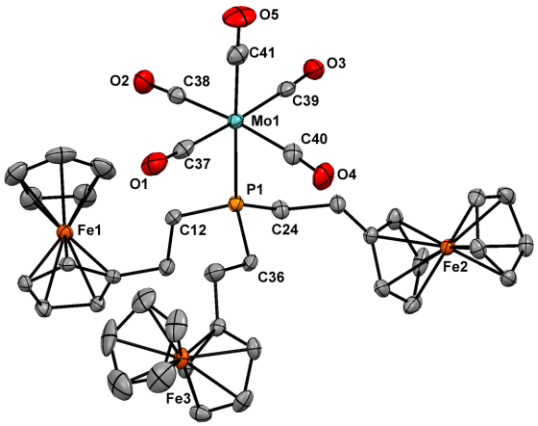

Fig. S35 Solid-state structure of **6c**. Anisotropic displacement ellipsoids are shown at 50% probability and hydrogen atoms have been omitted for clarity.

FT-IR absorption spectra

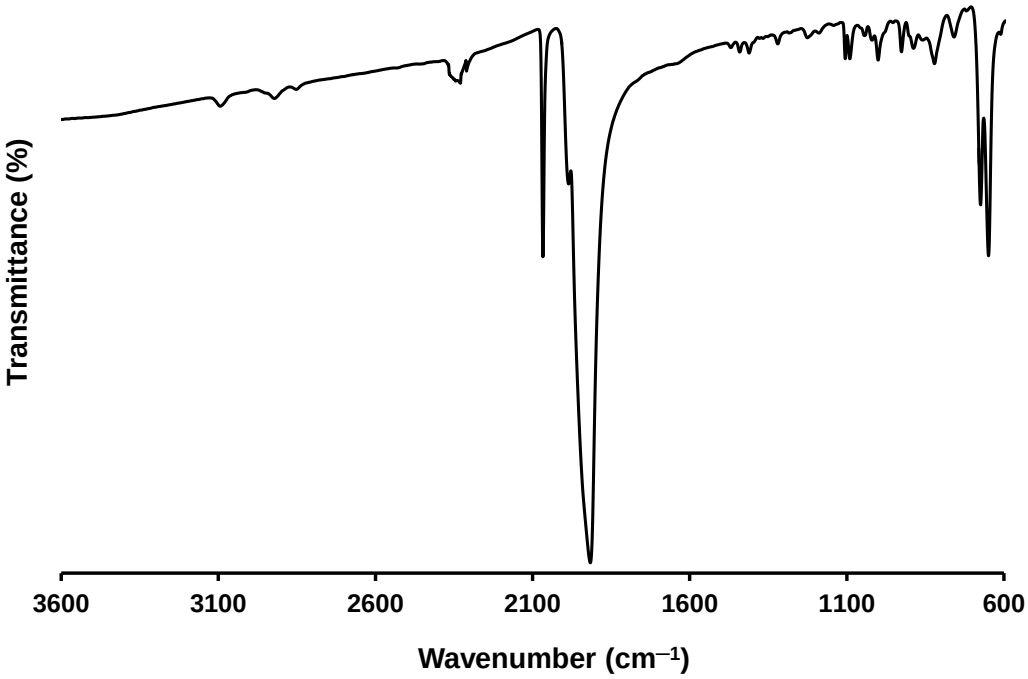

Fig. S36 FT-IR absorption spectrum of **5a** recorded as a thin film on a KBr plate.

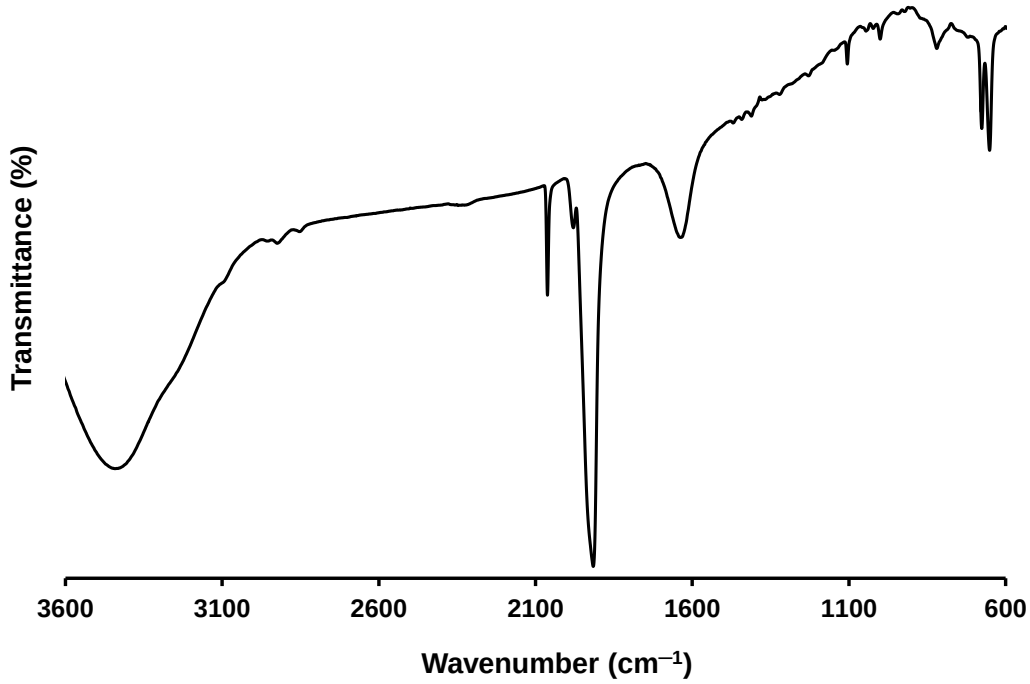

Fig. S37 FT-IR absorption spectrum of **5b** recorded as a thin film on a KBr plate.

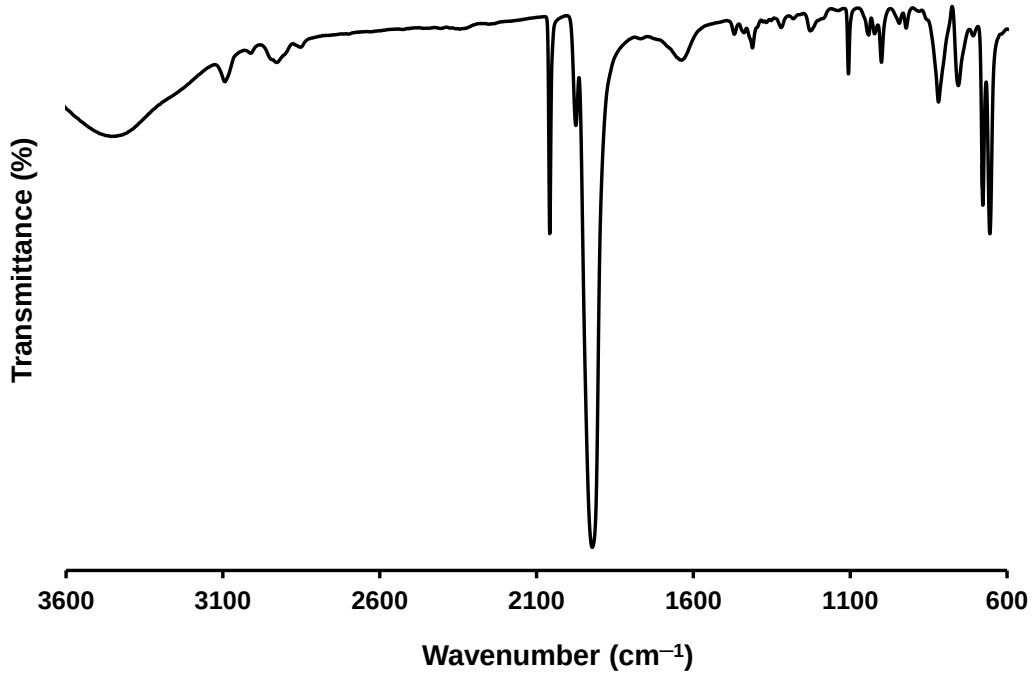

Fig. S38 FT-IR absorption spectrum of **5c** recorded as a thin film on a KBr plate.

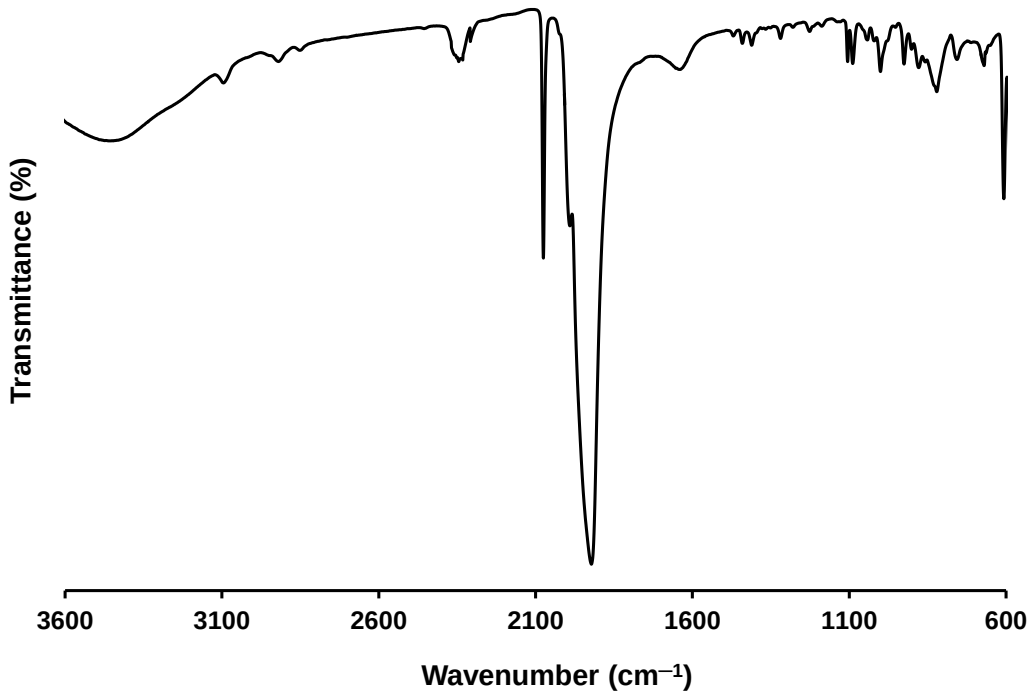

Fig. S39 FT-IR absorption spectrum of **6a** recorded as a thin film on a KBr plate.

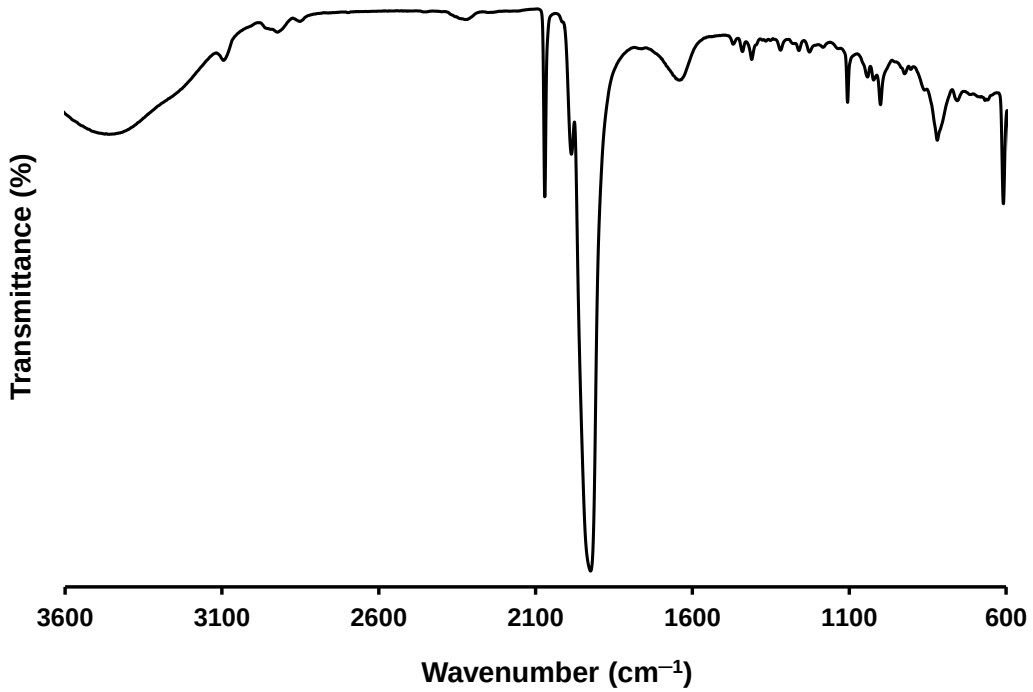

Fig. S40 FT-IR absorption spectrum of **6b** recorded as a thin film on a KBr plate.

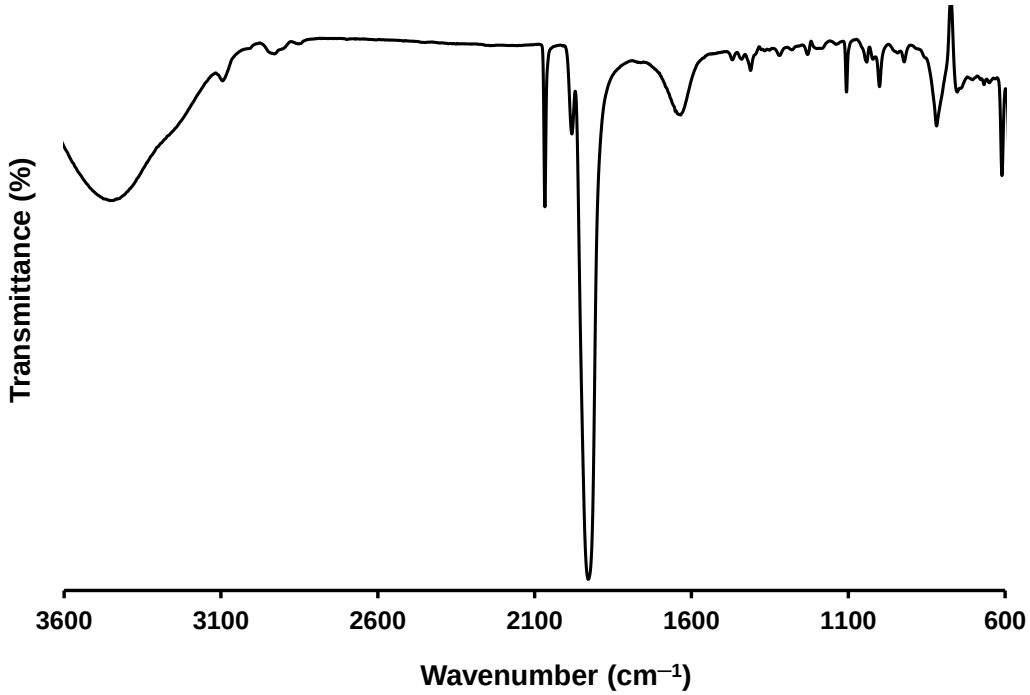

Fig. S41 FT-IR absorption spectrum of **6c** recorded as a thin film on a KBr plate.

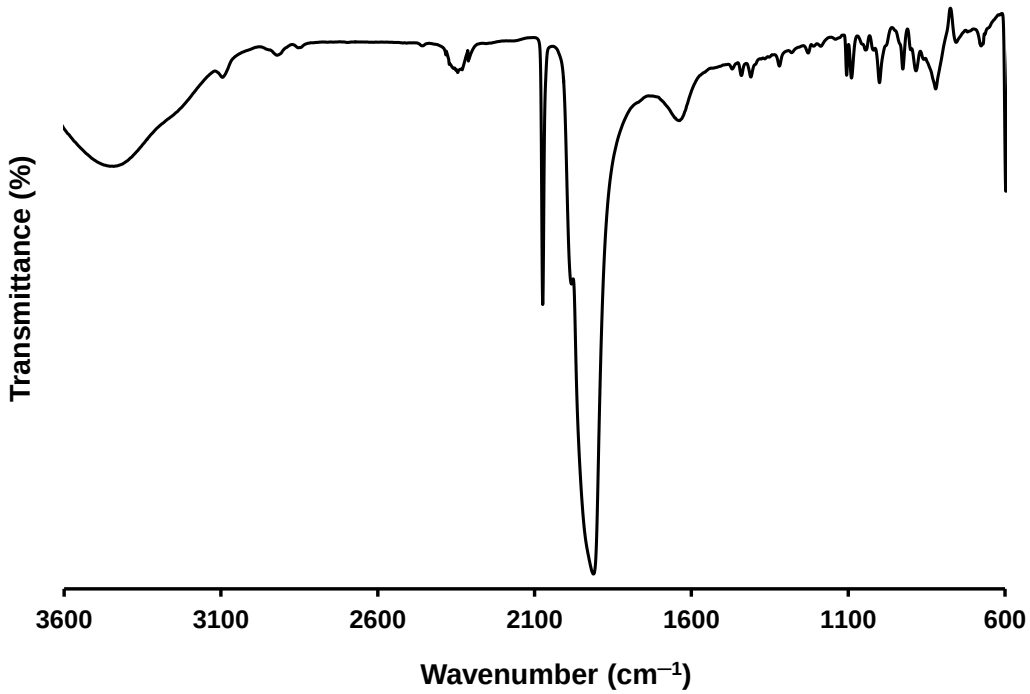

Fig. S42 FT-IR absorption spectrum of **7a** recorded as a thin film on a KBr plate.

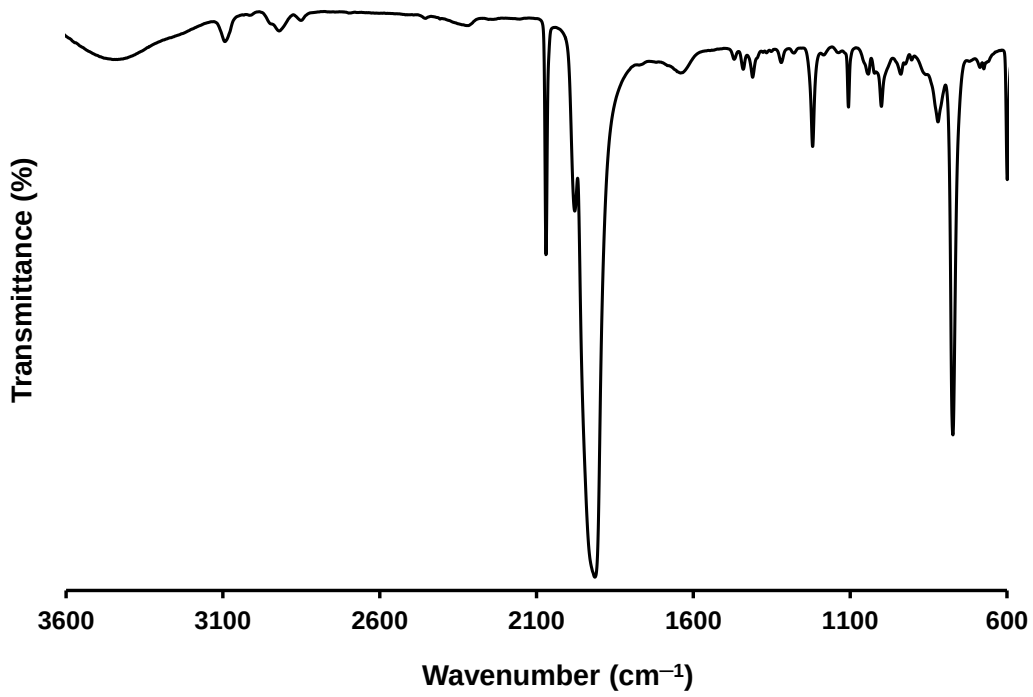

Fig. S43 FT-IR absorption spectrum of **7b** recorded as a thin film on a KBr plate.

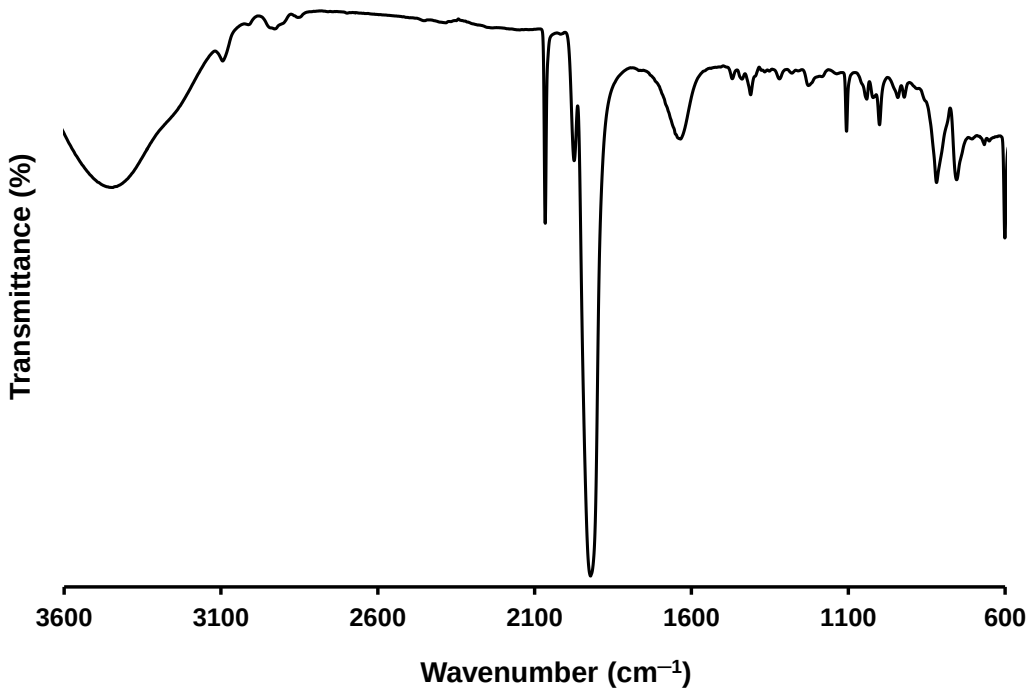

Fig. S44 FT-IR absorption spectrum of **7c** recorded as a thin film on a KBr plate.

UV-Vis Absorption Spectra

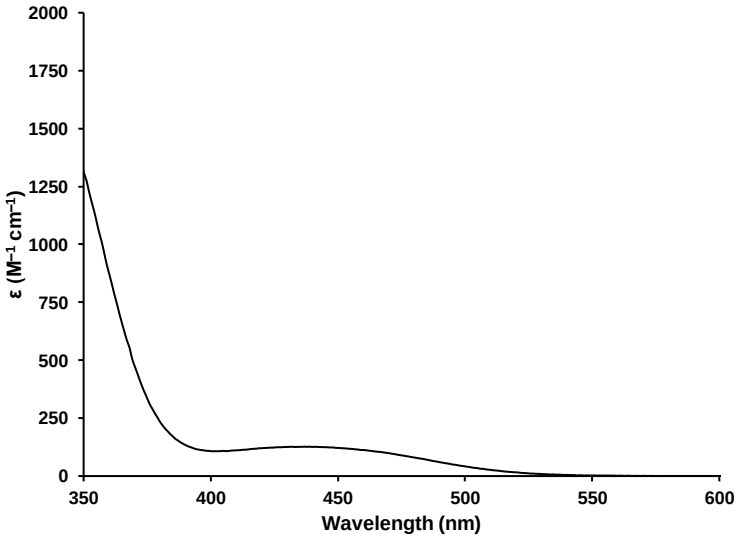

Fig. S45 UV-Vis absorption spectrum of **5a** recorded in CH_2Cl_2.

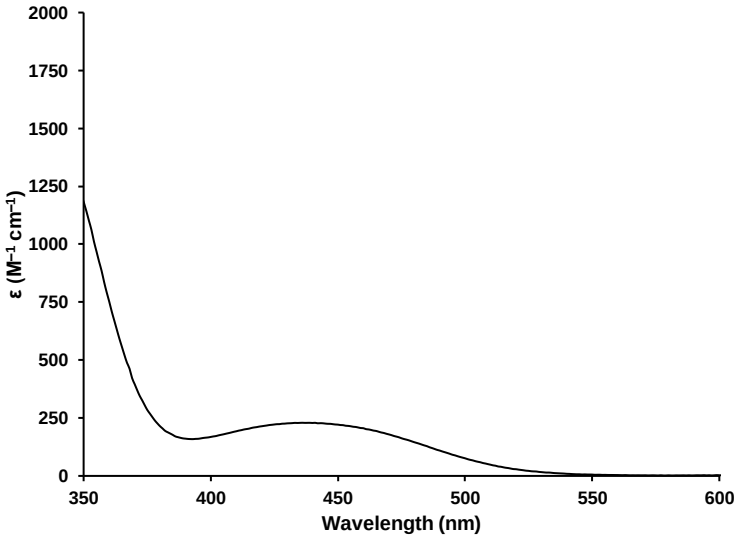

Fig. S46 UV-Vis absorption spectrum of **5b** recorded in CH_2Cl_2.

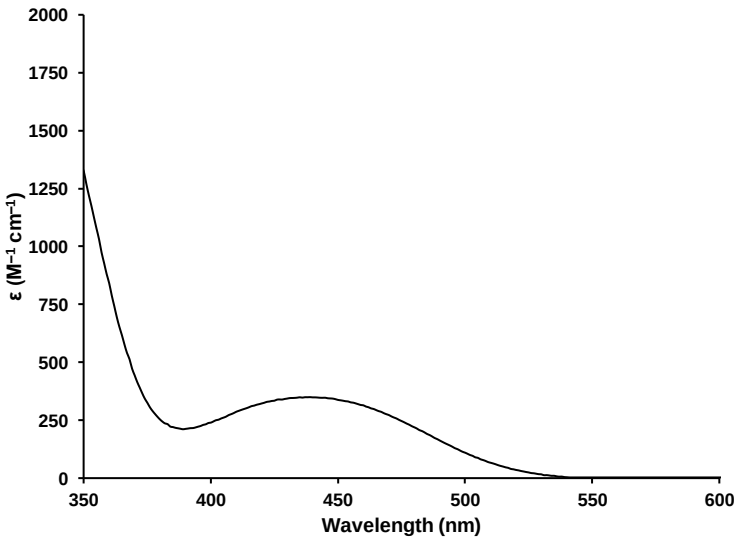

Fig. S47 UV-Vis absorption spectrum of **5c** recorded in CH_2Cl_2.

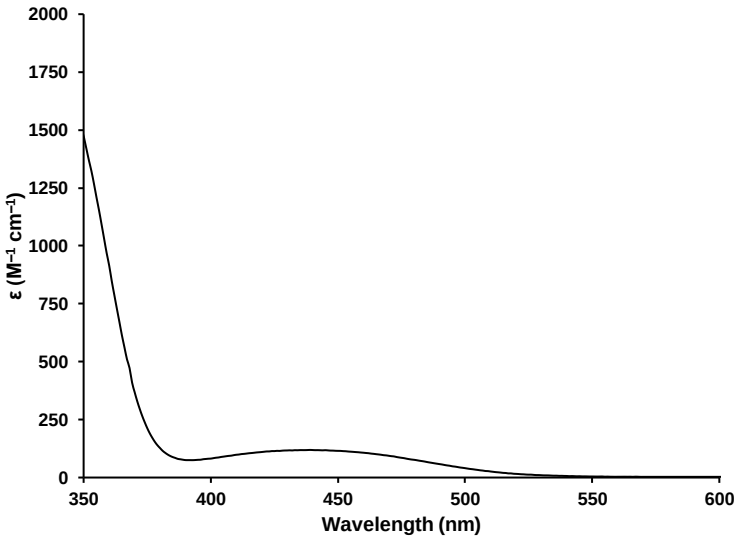

Fig. S48 UV-Vis absorption spectrum of **6a** recorded in CH_2Cl_2.

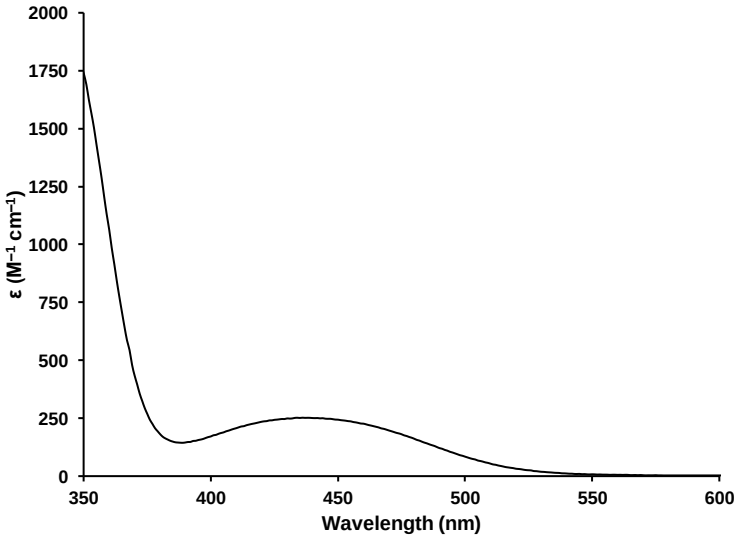

Fig. S49 UV-Vis absorption spectrum of **6b** recorded in CH_2Cl_2.

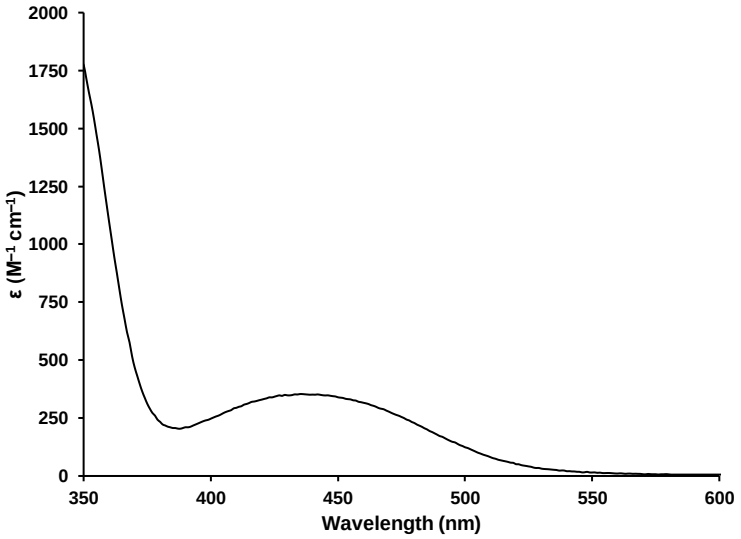

Fig. S50 UV-Vis absorption spectrum of **6c** recorded in CH_2Cl_2.

Cyclic Voltammograms

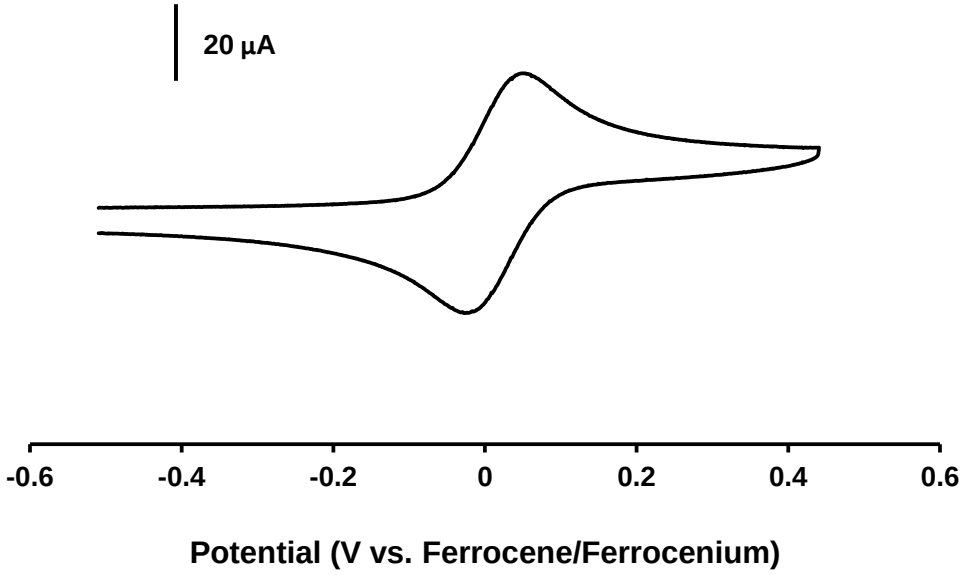

Fig. S51 Cyclic voltammogram of **5a** recorded at 250 mV s^{-1} for a 1 mM degassed 2:1 CH_2Cl_2:CH_3CN solution containing 0.1 M [*n*-Bu_4N][SO_3CF_3] as supporting electrolyte.

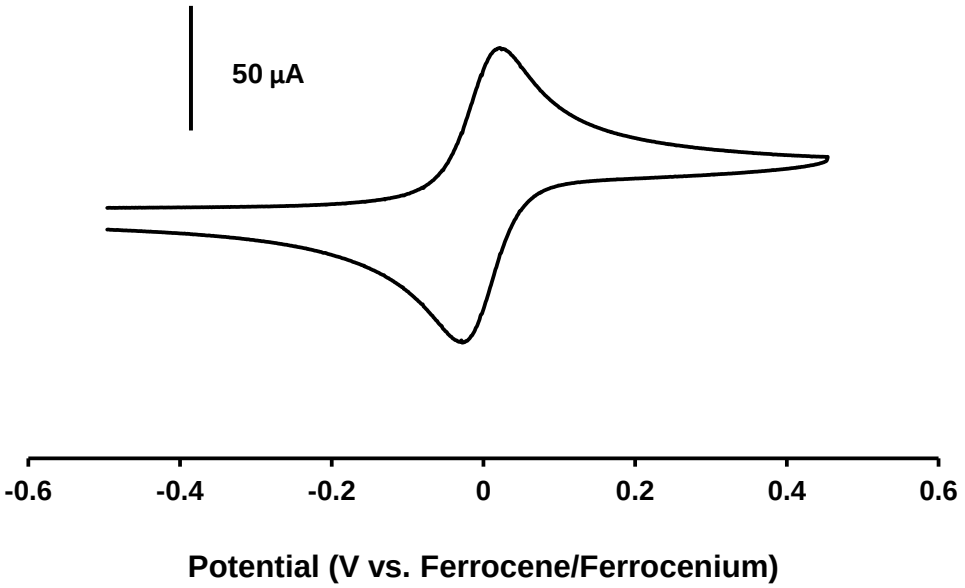

Fig. S52 Cyclic voltammogram of **5b** recorded at 250 mV s^{-1} for a 1 mM degassed 2:1 CH_2Cl_2:CH_3CN solution containing 0.1 M [*n*-Bu_4N][SO_3CF_3] as supporting electrolyte.

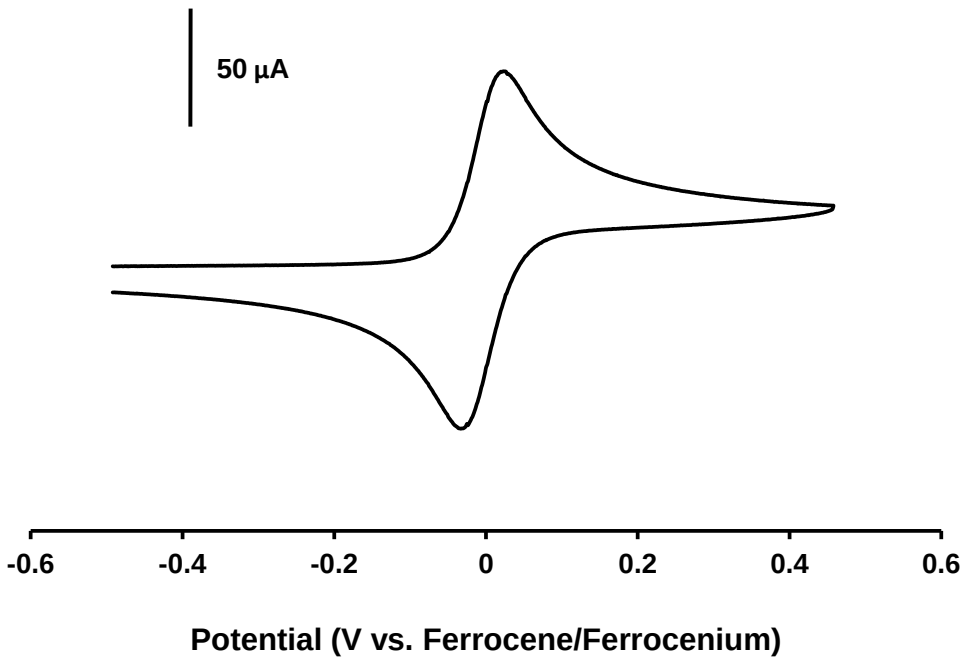

Fig. S53 Cyclic voltammogram of **5c** recorded at 250 mV s^{-1} for a 1 mM degassed 2:1 CH_2Cl_2:CH_3CN solution containing 0.1 M [*n*-Bu_4N][SO_3CF_3] as supporting electrolyte.

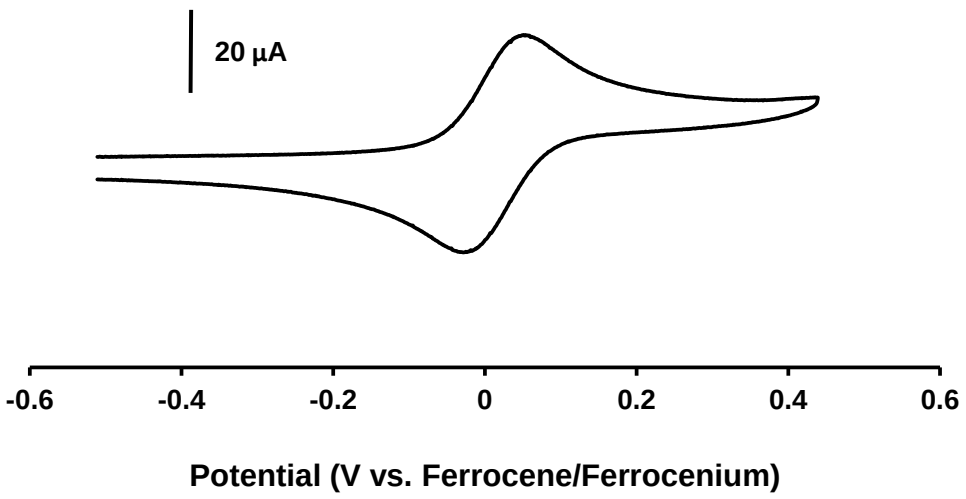

Fig. S54 Cyclic voltammogram of **6a** recorded at 250 mV s^{-1} for a 1 mM degassed 2:1 CH_2Cl_2:CH_3CN solution containing 0.1 M [*n*-Bu_4N][SO_3CF_3] as supporting electrolyte.

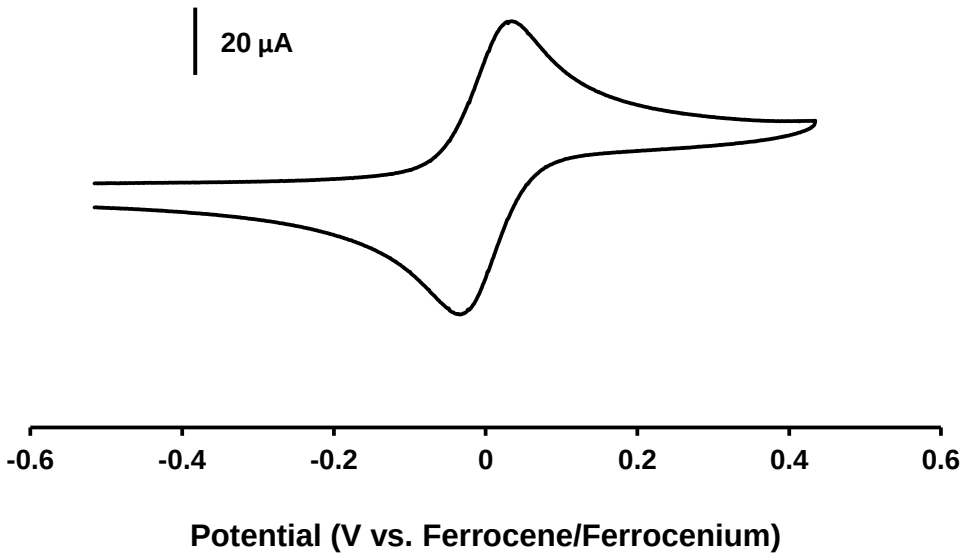

Fig. S55 Cyclic voltammogram of **6b** recorded at 250 mV s^{-1} for a 1 mM degassed 2:1 CH_2Cl_2:CH_3CN solution containing 0.1 M [*n*-Bu_4N][SO_3CF_3] as supporting electrolyte.

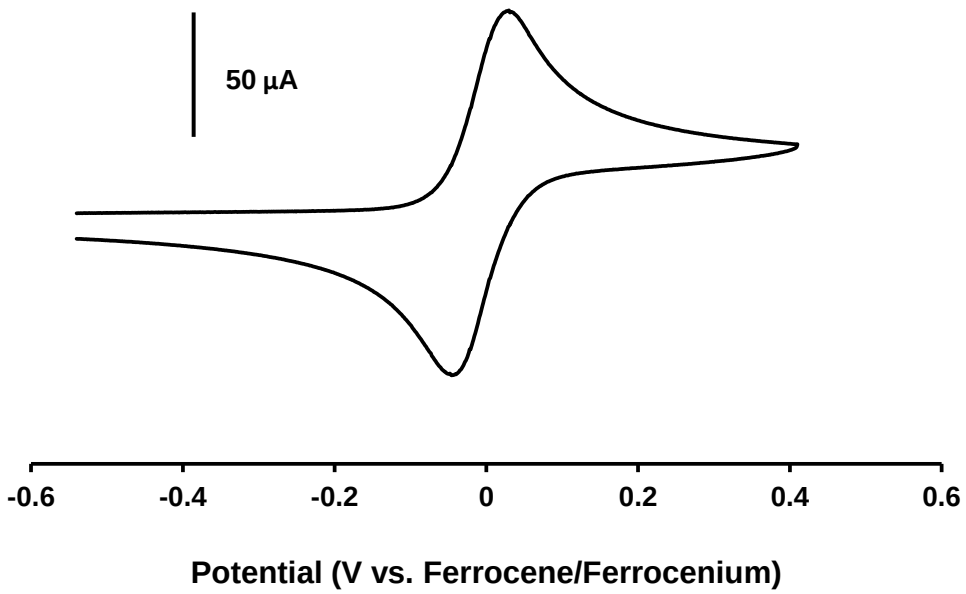

Fig. S56 Cyclic voltammogram of **6c** recorded at 250 mV s^{-1} for a 1 mM degassed 2:1 CH_2Cl_2:CH_3CN solution containing 0.1 M [*n*-Bu_4N][SO_3CF_3] as supporting electrolyte.

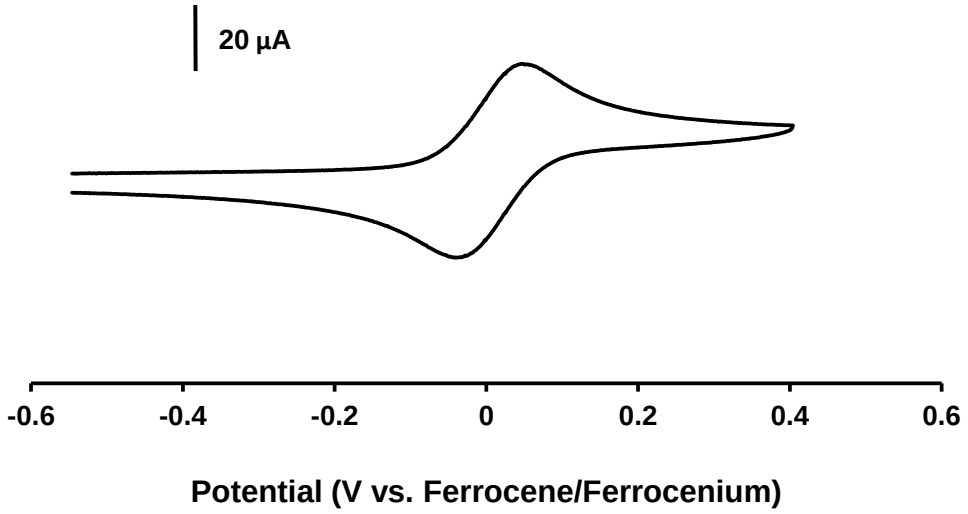

Fig. S57 Cyclic voltammogram of **7a** recorded at 250 mV s^{-1} for a 1 mM degassed 2:1 CH_2Cl_2:CH_3CN solution containing 0.1 M [*n*-Bu_4N][SO_3CF_3] as supporting electrolyte.

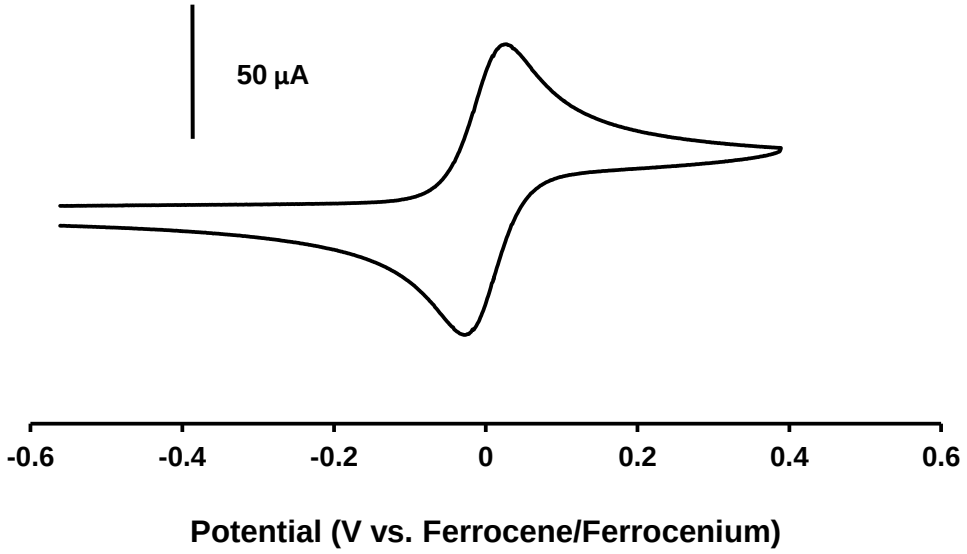

Fig. S58 Cyclic voltammogram of **7b** recorded at 250 mV s^{-1} for a 1 mM degassed 2:1 CH_2Cl_2:CH_3CN solution containing 0.1 M [*n*-Bu_4N][SO_3CF_3] as supporting electrolyte.